JNC TN8400 99-031

COUPLED THERMO - HYDRO - MECHANICAL EXPERIMENT AT KAMAISHI MINE

TECHNICAL NOTE 16-99-03

ANALYSES OF TASK 2C, DECOVALEX II

M. Chijimatsu and T. Fujita
Japan Nuclear Cycle Development Institute (JNC)
A. Kobayashi
Iwate University
Y. Ohnishi
Kyoto University

JNC TN8400 99-031
1999年6月

釜石原位置試験場における粘土充填・熱負荷試験
テクニカルノート 16-99-03
DECOVALEX Task 2C の解析結果
(研究報告)

千々松正和*1・藤田朝雄*1・小林晃*2・大西有三*3

要　旨

地層処分における技術開発の観点からは，工学規模での試験によるニアフィールド環境である周辺岩盤の挙動が人工バリアに与える影響の把握および周辺岩盤を含むニアフィールド性能の定量的評価と室内および原位置における大型試験による人工バリアの品質性能の確認を行い，地層処分技術の信頼性向上を図ることが重要となっている。そのため，核燃料サイクル開発機構東海事業所の地層処分基盤研究施設等における工学規模の試験と並行して，原位置試験場において，人工バリアの品質性能の確認およびその実岩盤条件下でのニアフィールド連成挙動を評価することが必要となっている。そこで，実条件でのニアフィールド環境を把握するため釜石原位置試験場において粘土充填・熱負荷試験を実施した。本試験結果は、国際共同研究DECOVALEXの解析課題の一つ（Task 2）となっている。Task 2はSubtask A,B,Cの３段階に分けられており，順次解析を実施していくこととなっている。本論では，このうちサイクル機構が実施したSubtask Cの解析結果について報告する。Subtask Cは粘土充填・熱負荷試験における連成試験の解析評価であり，人工バリア内の解析であるSubtask C1とニアフィールド岩盤を含めた解析であるSubtask C2からなっている。Subtask C2に関しては原位置で得られた試験結果との比較を行なった。サイクル機構において開発された連成解析モデルによる解析により，原位置において生じた現象をほぼ再現することができた。

---

*1 東海事業所　環境保全・研究開発センター
処分研究部　処分バリア性能研究グループ
*2 岩手大学　農学部
*3 京都大学　工学部

COUPLED THERMO-HYDRO-MECHANICAL EXPERIMENT AT KAMAISHI MINE

TECHNICAL NOTE 16-99-03

ANALYSES OF TASK 2C, DECOVALEX II

ABSTRACT

It is an important part of the near field performance assessment of nuclear waste disposal to evaluate coupled thermo-hydro-mechanical (T-H-M) phenomena, e.g., thermal effects on groundwater flow through rock matrix and water seepage into the buffer material, the generation of swelling pressure of the buffer material, and thermal stresses potentially affecting porosity and fracture apertures of the rock. An in-situ T-H-M experiment named 'Engineered Barrier Experiment' has been conducted at the Kamaishi Mine, of which host rock is granodiorite, in order to establish conceptual models of the coupled T-H-M processes and to build confidence in mathematical models and computer codes.

The coupled T-H-M experiment is one of tasks in DECOVALEX (**DE**velopment of **CO**upled models and their **VAL**idation against **EX**periments) project which is an international co-operative project and it is defined as Task 2. The Task 2 for the DECOVALEX project are divided into three subtasks (A-C) in accordance with the programme and availability of data, called subtasks.

This note describes the results of subtask C. Subtask C is a coupled thermo-hydro-mechanical analysis in the near field.

COUPLED THERMO-HYDRO-MECHANICAL EXPERIMENT AT KAMAISHI MINE

TECHNICAL NOTE 16-99-03

ANALYSES OF TASK 2C , DECOVALEX II

CONTENTS

List of Figures

List of Tables

1. Introduction

Japan Nuclear Cycle Development Institute (JNC) has conducted the activities of geoscientific R&D program. In order to understand the deep geological condition in fractured crystalline rock, JNC initiated the in-situ experiments in the Kamaishi Mine, where early Cretaceous granodiorite hosts the experiments [Takeda, S. and Osawa, H., 1993] [Yamato, A., et al., 1992].

The coupled thermo-hydro-mechanical (T-H-M) experiment in situ has been carried out as a task of the Kamaishi in-situ experiments in order to establish the coupled T-H-M conceptual models and to build up confidence to the mathematical models and computer codes. The program of T-H-M experiment is divided into five phases; Excavation of Drifts, Measurement of Rock Properties, Excavation of Test Pit, Setting up of Bentonite, and T-H-M test [Fujita, T., et al., 1994]. T-H-M model has been developed by JNC for the evaluation of coupled T-H-M behaviors in the near field, and then this model is applied to the results of Kamaishi in-situ experiment.

The coupled T-H-M experiment is one of tasks in DECOVALEX (**DE**velopment of **CO**upled models and their **VAL**idation against **EX**periments) project which is an international co-operative project, initiated by Swedish Nuclear Power Inspectorate (SKI) and it is defined as Task 2. The Task 2 for the DECOVALEX project are divided into three subtasks (A-C) in accordance with the program and availability of data, called subtasks.

- Subtask A (Task 2A):
  - 1: Prediction of fracture distribution pattern in the rock surface of the test pit.
  - 2: Prediction of inflow into the test pit.
  - 3: Prediction of mechanical effects on the rock surrounding the test pit.
  - 4: Prediction of pore pressure in the rock surrounding the test pit.
- Subtask B (Task 2B):
  - 1: Calibration of Task 2A.
- Subtask C (Task 2C):
  - 1: Predictions of coupled T-H-M behavior of the buffer.
  - 2: Prediction of coupled T-H-M behaviors of the rock and the buffer.

Subtask A and B were carried out by using various methods and results of those were described in technical notes. [Fujita, T., et al., 1997a] [[Fujita, T., et al., 1998]

This report describes the results of Subtask C.

2. Task Definition

TASK 2C focuses on the coupled T-H-M phenomenon in the near field. The major objectives for the TASK 2C are to build up confidence to the coupled T-H-M models.

2.1 Task 2C-1

Task 2C-1 is a calculation of coupled T-H-M behavior of the buffer material with simple boundary conditions. The objective of TASK 2C-1 is to compare the models of the participants on coupled T-H-M phenomenon for buffer material. The coupled T-H-M calculations are carried out by two kinds of hydraulic boundary condition for buffer material as follows.

(a) Zero water flux at all outer boundaries of buffer material

An effect on temperature to water behavior and thermal stress in the buffer material is studied.

(b) Constant total head at all outer boundaries of buffer material except for the top which has zero water flux

This calculation is similar to BIG-BEN experiment and focuses on not only water behavior and thermal stress but swelling pressure.

The mechanical and thermal boundary conditions for the model are given as :

- Mechanical boundary conditions :

  All boundaries are fixed by zero displacements in the normal and horizontal directions.

- Thermal boundary conditions :

  The top boundary of the lid is fixed by a constant temperature. The heat transfer condition is imposed on the other boundaries.

  Heat transfer coefficient = 10.0 W/(m^2•°C)

The models on TASK 2C-1 are presented in Figure 2-1.

2.2 Task 2C-2

Task 2C-2 is a prediction of coupled T-H-M behavior of both the rock and buffer material. TASK 2C-2 focuses on full bentonite and rock system. The example of model on TASK 2C-2 is presented in Figure 2-2.

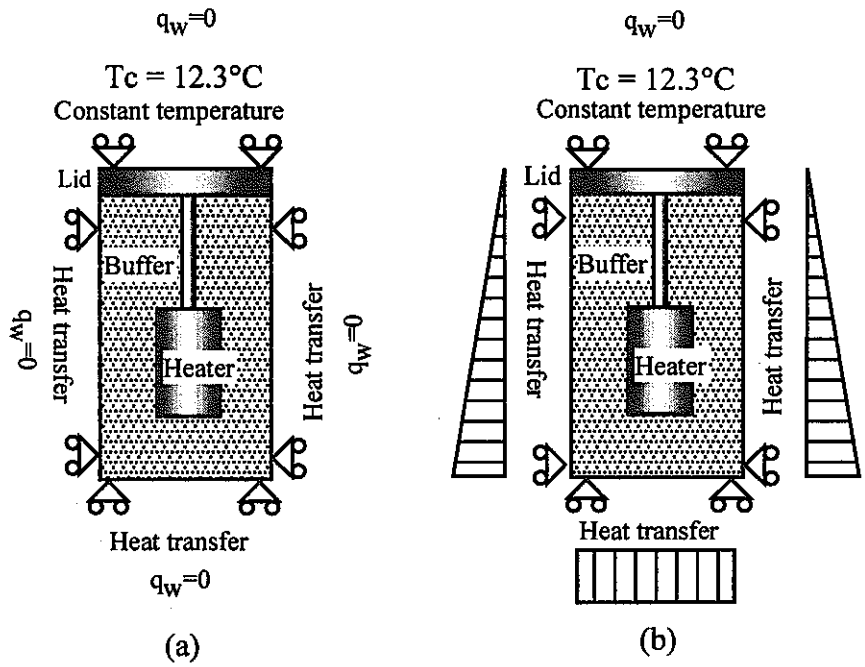

Figure 2-1 Models on TASK 2C-1

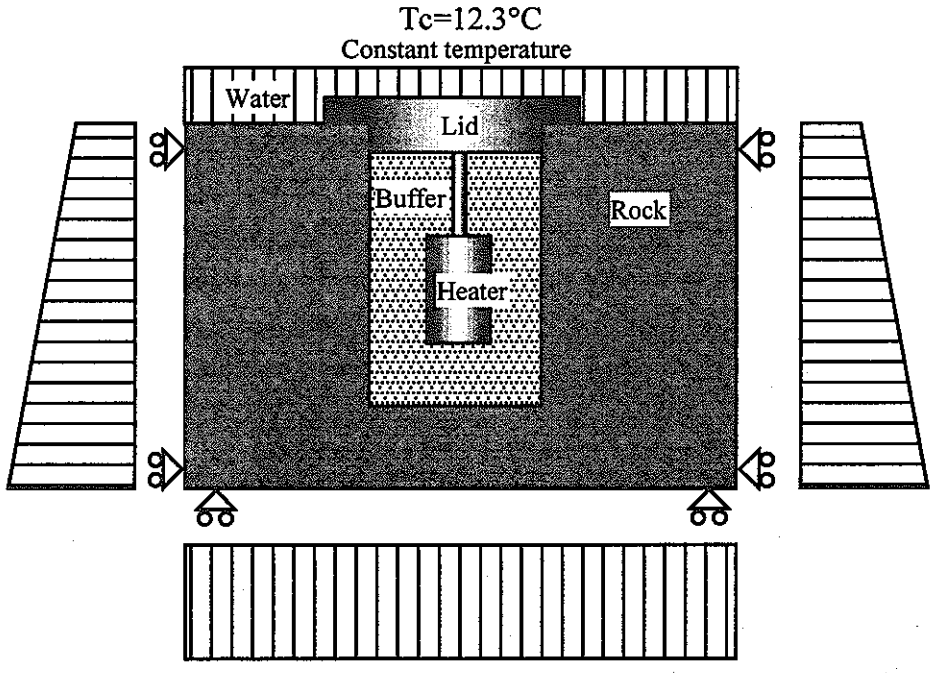

Figure 2-2 Example of model on TASK 2C-2

3. Analysis code

3.1 Outline

Analysis of the coupled thermo-hydro-mechanical process is carried out with the computer code named THAMES [Ohnishi, Y., et al, 1989]. THAMES is a finite element code for analysis of coupled T-H-M behaviors of a saturated - unsaturated medium. THAMES is extended to take account of the behavior in the buffer material such as the water flow due to thermal gradient and the swelling phenomena [Stephansson, O., 1995]. The unknown variables are total pressure, displacement vector and temperature. The quadratic shape function is used for the displacements and linear one is used for total pressure and temperature.

3.2 Governing Equation of Coupled T-H-M Process

The behavior of the buffer material is influenced by the interdependence of thermal, hydraulic and mechanical phenomena. To treat the water/vapor movement [Philip, J.R. and de Vries, D.A, 1957] and heat induced water movement[de Vries, D.A, 1974], the continuity equation used in the extended THAMES code is as follows;

$$\left\{\xi\rho_l D_\theta \frac{\partial\theta}{\partial\psi}(h_{,i}-z_{,i})+(1-\xi)\frac{\rho_l{}^2 gK}{\mu_l}h_{,i}\right\}_{,i}+\{\rho_l D_T T_{,i}\}_{,i}$$
$$-\rho_{l0}nSr\rho_l g\beta_P\frac{\partial h}{\partial t}-\rho_l\frac{\partial\theta}{\partial\psi}\frac{\partial h}{\partial t}-\rho_l Sr\frac{\partial u_{i,i}}{\partial t}+\rho_{l0}nSr\beta_T\frac{\partial T}{\partial t}=0 \qquad (1)$$

where D_θ is the isothermal water diffusivity, θ is the volumetric water content, ψ is the water potential head and K is the intrinsic permeability. ξ is the unsaturated parameter, $\xi = 0$ at the saturated zone, $\xi = 1$ at the unsaturated zone. μ_l is the viscosity of water, ρ_l is the density of water, g is the gravitational acceleration. D_T is the thermal water diffusivity, n is the porosity, S_r is the degree of saturation, β_P is the compressibility of water, β_T the thermal expansion coefficient of water, z is the elevation head. u_i is the displacement vector, T is the temperature, h is the total head and t is the time. The subscript, 0, means the reference state.

This equation means that the water flows in the unsaturated zone is expressed by diffusion equation and in the saturated zone by Darcy's law.

The energy conservation equation has to treat the energy change by evaporation. The equation is given as

$$(\rho C_v)_m \frac{\partial T}{\partial t} + nSr\rho_l C_{vl} V_l T_{,i} - K_{Tm} T_{,ii} + L\left\{ D_{\theta v} \frac{\partial \theta}{\partial \psi}(h_{,i} - z_{,i}) \right\}_{,i}$$
$$+ nSrT \frac{\beta_T}{\beta_P} \left\{ \xi D_\theta \frac{\partial \theta}{\partial \psi}(h_{,i} - z_{,i}) + (1-\xi)\frac{\rho_l g K}{\mu_l} h_{,i} + D_T T_{,i} \right\}_{,i} \qquad (2)$$
$$+ \frac{1}{2}(1-n)\beta T \frac{\partial}{\partial t}(u_{i,j} + u_{j,i})\delta_{ij} = 0$$

where $(\rho C_v)_m$ is the specific heat of the material consisting of water and the soil particles, C_{vl} is the specific heat of water, V_l is the velocity vector of water, K_{Tm} is the thermal conductivity of consisting of water and the solid particles, L is the latent heat of vaporization per unit volume and $D_{\theta v}$ is the water vapor diffusivity which will be explained in the following section.

The equilibrium equation has to take the swelling behavior into account.

$$\left[\frac{1}{2} C_{ijkl}(u_{k,l} + u_{l,k}) - F\pi\delta_{ij} - \beta\delta_{ij}(T - T_0) + \chi\delta_{ij}\rho_l h \right] + \rho b_i = 0 \qquad (3)$$

where C_{ijkl} is the elastic matrix, ρ is the density of the medium, b_i is the body force. χ is the parameter for the effective stress, $\chi = 0$ at the unsaturated zone, $\chi = 1$ at the saturated zone. F is the coefficient relating to the swelling pressure process. β is defined as

$$\beta = (3\lambda + 2\mu)\,\alpha_s \qquad (4)$$

where λ and μ are Lame's constants and α_s is the thermal expansion coefficient.

π is the swelling pressure. The swelling pressure can be assumed the function of water potential head (ψ) as follows;

$$\pi(\theta_1) = \rho_l g(\Delta\psi) = \rho_l g(\psi(\theta_1) - \psi(\theta_0)) = \rho_l g \int_{\theta_0}^{\theta_1} \frac{\partial \psi}{\partial \theta} d\theta \qquad (5)$$

where θ_0 is the volumetric water content at the initial state.

This is based on the theory that swelling pressure is equivalent to the water potential [Nakano, M., et al., 1984].

4. Fundamental Properties of Buffer Material

The buffer material used in the experiment is a granulated bentonite, BENTONITE OT-9607[Fujita, T., et al., 1997b]. Figure 4-1 (a) shows the equipment for the infiltration experiment. The compacted specimen is set in the stainless steel cell and water is supplied to the specimen from the bottom. In this experiment, specimen is sliced into 2 mm sections after various diffusion periods and volumetric water content of each specimen is measured by the oven-drying method. The water diffusivity is calculated by the following equation based on the distribution on volumetric water content obtained by the experiment [Philip, J.R. and de Vireos, DA, 1957].

$$D_\theta = \frac{\int_{zi}^{l}(\theta_{t=t_2} - \theta_{t=t_1})dz}{\frac{1}{2}\left\{\left(\frac{\partial\theta}{\partial z}\right)_{\substack{t=t_2\\z=zi}} + \left(\frac{\partial\theta}{\partial z}\right)_{\substack{t=t_1\\z=zi}}\right\}} \times \frac{1}{t_2 - t_1} \tag{6}$$

where t is infiltration time, l is the length of the specimen and zi ($0 \leqq zi \leqq l$) is distance from the bottom of the specimen.

Figure 4-1(b) shows the measured isothermal water diffusivity of the buffer material with the dry density of 1.65g/cm^3. Under unsaturated conditions, water movement within the buffer material has often been expressed as a simple diffusion model with constant apparent water diffusivity. However, such a simple model is rather conceptual and the water content dependence of the water diffusivity has not been examined yet. Water movement in unsaturated porous media is known as a transfer process in both vapor and liquid phase. Therefore, it is necessary to take the two-phase contribution into consideration in the modeling. As shown in Figure 4-1(b), the water diffusivity is obtained as functions of water content and temperature. The water movement behavior is examined by applying the Philip & de Vireos' [Philip, J.R. and de Vireos, DA, 1957] and Drake's equations to the obtained water diffusivities. The effect of temperature on water diffusivity is examined by separating the contributions of the vapor and liquid phase. The Philip and de Vireos' equation under isothermal condition is expressed as

$$D_{\theta v} = a\tau D_a \nu \rho^* h_r g \frac{1}{\rho_l}\frac{M}{RT}\frac{\partial\psi}{\partial\theta} \tag{7}$$

and Drake's equation is expressed as

$$D_{\theta l} = k\frac{\partial\psi}{\partial\theta} \tag{8}$$

where $D_{\theta v}$ is the water vapor diffusivity under isothermal condition, a is the air filled porosity, τ is the tortuousity, D_a is the diffusion coefficient for water vapor in air, ν is the mass flow factor, ρ^* is the density of saturated water vapor, h_r is the relative humidity. $D_{\theta l}$ is the liquid water diffusivity and k is the unsaturated hydraulic conductivity for liquid phase. The mass flow factor is calculated from

$$\nu = P_T / (P_T - P) \tag{9}$$

where P_T is the total gas pressure. Values of the diffusion coefficient for water vapor, D_a, and the density of saturated water vapor, ρ^*, are given from the literature. The relative humidity, h_r, is obtained by the psychrometric measurement.

The calculated results can show good agreement with the experimental ones [Takeuchi, S., et al, 1995]. Thus, the temperature dependence of the water diffusivity can also be explained by Philip and de Vreis' equation and Drake's equation. However, because some parameters are difficult to identify. Therefore, for the simulation, an approximation function is applied as water diffusivity as shown in next section.

The water potential heads of specimen with various water content are measured by the thermocouple psychrometer. Figure 4-2(a) shows the thermocouple psychrometer sample changer by Decagon Device inc., USA [Decagon Device Inc.]. The psychrometer senses the relative humidity of vapor in equilibrium with the liquid phase in the specimen. Figure 4-2(b) shows the relations between the water potential head and the volumetric water content. It is appears from this figure that the water potential head is not affected by temperature.

Figure 4-3(a) shows the equipment for the swelling pressure measurement. The compacted specimen is set in the stainless steel cell and water is supplied to the specimen from the bottom. The swelling pressure is measured by pressure cell. The result of the swelling pressure measurement is presented in Figure 4-3(b). The curve shows a stabilization point at around 0.95 MPa.

Young's modulus, unconfined compressive strength and thermal conductivity are measured as a function water content as shown in Figures 4-4, 4-5 and 4-6.

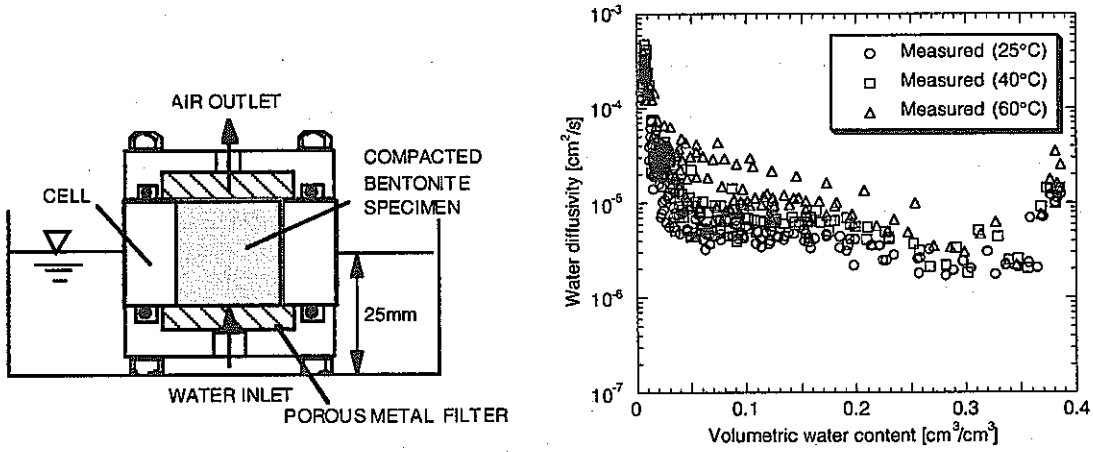

(a) (b)

Figure 4-1 Equipment for infiltration experiment (a) and relationship between isothermal water diffusivity and volumetric water content (b)

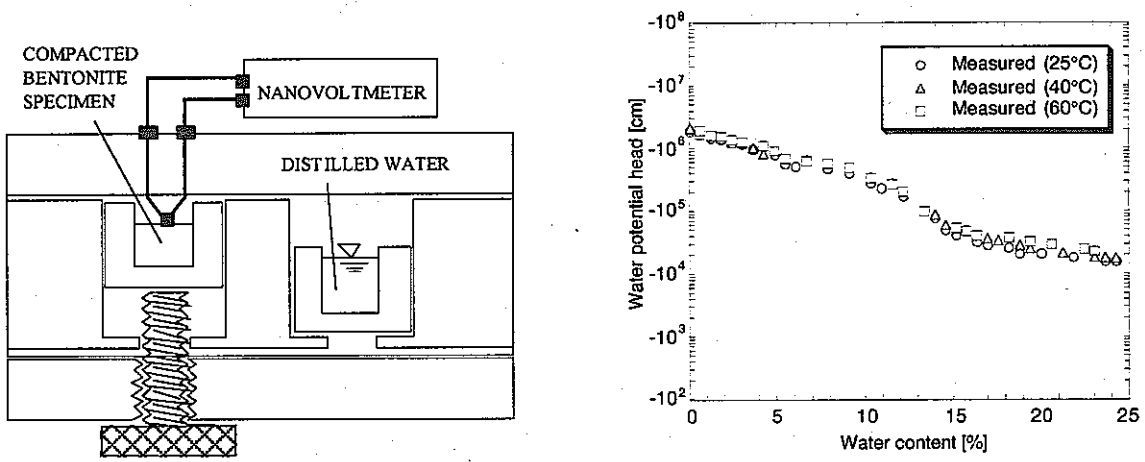

(a) (b)

Figure 4-2 Thermocouple psychrometer sample changer (a) and relationship between water potential head and water content (b)

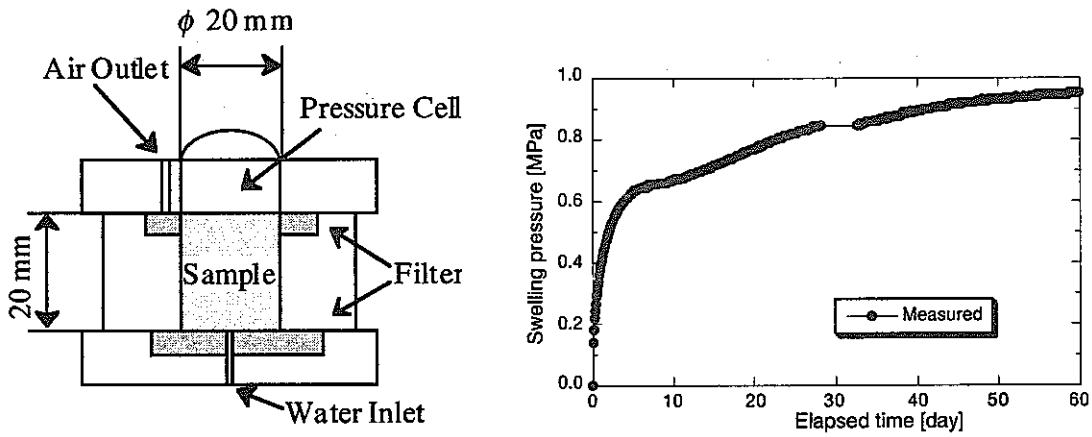

(a) (b)

Figure 4-3 Equipment for swelling pressure measurement (a) and time history of swelling pressure

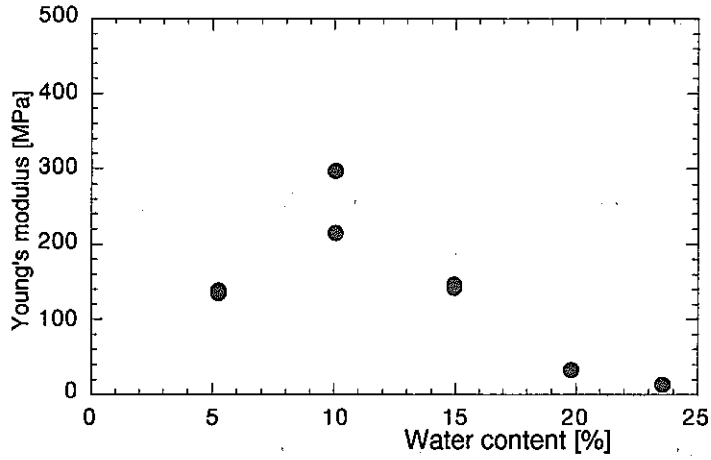

Figure 4-4 Relationship between Water content and Young's modulus

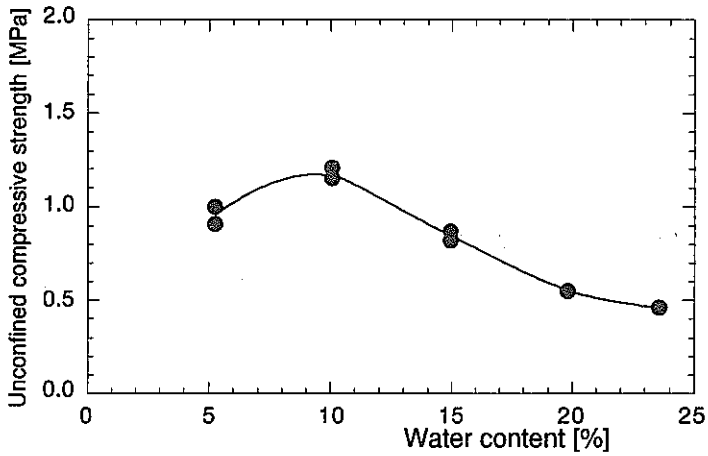

Figure 4-5 Relationship between Water content and Unconfined compressive strength

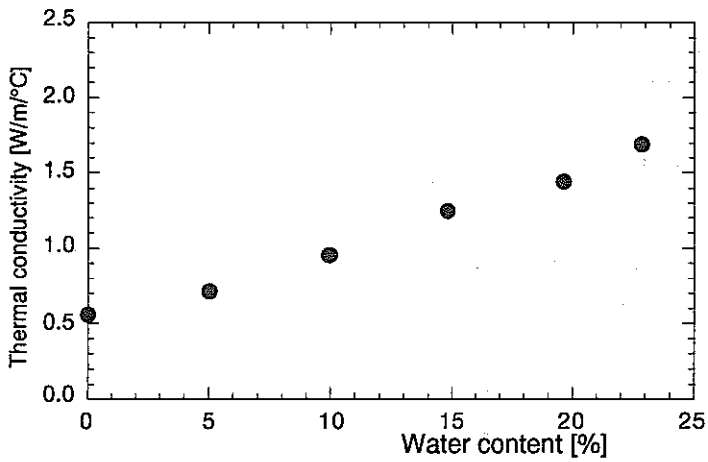

Figure 4-6 Relationship between Water content and Thermal conductivity

5 Parameter Identification

5.1 Water Diffusivity

It is assumed in the model that the water diffusivity D_θ is expressed the sum of vapor phase diffusivity $D_{\theta v}$ and liquid phase diffusivity $D_{\theta l}$.

$$D_\theta = D_{\theta v} + D_{\theta l} \tag{10}$$

Water moves in the vapor phase at the dry condition and in the liquid phase at the wet condition [Takeuchi, S., et al.,1995]. Therefore, vapor phase diffusivity and liquid phase diffusivity are defined as

$$\lim_{\theta \to \theta s} D_{\theta v} = 0 \tag{11}$$

$$\lim_{\theta \to 0} D_{\theta l} = 0 \tag{12}$$

where, θ_s is the saturated volumetric water content.

A hyperbolic function (12) is used for the water diffusivity. [Suzuki, H., et al., 1995]

$$f(\theta) = \frac{a}{\theta - b} + c \tag{12}$$

From the equations (11), (12) and (13), vapor phase diffusivity and liquid phase diffusivity are expressed as

$$D_{\theta v}(\theta) = \frac{a_1(\theta - \theta_s)}{(\theta - b_1)(b_1 - \theta_s)} \tag{14}$$

$$D_{\theta l}(\theta) = \frac{a_2 \theta}{b_2(\theta - b_2)} \tag{15}$$

where, a_1, a_2, b_1 and b_2 are the coefficients.

Therefore, the water diffusivity is expressed as

$$D_\theta(\theta) = \frac{a_1(\theta - \theta_s)}{(\theta - b_1)(b_1 - \theta_s)} + \frac{a_2 \theta}{b_2(\theta - b_2)} \tag{16}$$

The coefficients are obtained from the fitting of data measured at each temperature. The coefficients are given as a function of temperature as shown in the following equations.

$$a_1 = 3.68\times10^{-8}T - 2.08\times10^{-7} \quad (17)$$

$$a_2 = -3.58\times10^{-9}T - 2.19\times10^{-7} \quad (18)$$

$$b_1 = -1.00\times10^{-3} \quad (19)$$

$$b_2 = 0.41 \quad (20)$$

$$\theta_s = 0.389 \quad (21)$$

where, T is the temperature.

Figure 5-1 shows the water diffusivity by equation (6) (noted as Measured) and the one modeled by equation (16) (noted as Function).

5.2 Water Retention Curve

The relation between the water potential and the water content is called the water retention curve. This relation is very important for the unsaturated flow. The water potential was determined from the relative humidity and the water content was determined by the weight loss during a subsequent oven drying. The results of the experiments are presented in Figure 5-2. The results show that the water retention is essentially independent of the temperature. For the numerical simulation, the real experimental values are used as tabular except at full saturation where the water potential is set to 0. Figure 5-2 shows the measured water potential head and water retention curve that is used for simulation.

The infiltration test is simulated using the water diffusivity in Figure 5-1 and the water retention curve in Figure 5-2 in various temperatures. Figure 5-3 shows the comparisons between measured data and simulated results. In each temperature, calculated results show good agreement with measured results.

5.3 Thermal Water Diffusivity

The thermal water diffusivity D_T of buffer is evaluated with the result of the KID-BEN equipment. Figure 5-4 shows the schematic view of KID-BEN equipment. The infiltration test under thermal gradient condition is carried out in order to understand the behavior of the water movement in the unsaturated bentonite. The compacted specimen (diameter 50.0 mm, height 100.0 mm) packaged in a food wrap film is set in the apparatus. The cell of KID-BEN is made of Bakelite that is thermosetting resin, and the air layer that enhances heat-insulating effects. The system of the experiment is completely closed. The cooling and heating portions are composed of copper plates and thermostat with circulation system. The experiment is carried out with two specimens. One is used to obtain the temperature distribution and the other is used to obtain the water content distribution. In the first apparatus, the thermocouples are set from the holes into the specimen as shown in Figure 5-4. The specimen in the second apparatus is

sliced by 20 mm thickness after various infiltration periods. The water content of each sliced specimen is measured by oven-drying method. Temperature is fixed to be 40°C and 60°C at the top and bottom surface of specimen respectively. Initial water content of specimen is 16.5 % and infiltration periods id 400 hours.

The thermal water diffusivity is assumed as a function of temperature as follows;

$$D_T = D_{T0} \exp\left(\alpha \frac{T - T_0}{T_0} \right) \tag{25}$$

The parameters of equation (25) are estimated as equations (26)-(28) based on back analysis of KID-BEN test. At that time, heat transfer boundary conditions along the walls of the specimen were applying to simulate the heat loss through the walls of the test apparatus. The heat transfer coefficient at the boundaries was calibrated to 2.5 W/m^2°C assuming the environment temperature of 25°C. Figure 5-5 shows the comparison of water content distribution between measured data and calculated value.

$$D_{T0} = 8.5 \times 10^{-8} \text{ cm}^2/(\text{s °C}) \tag{26}$$

$$\alpha = -1.5 \ (T<60°C), \ 1.5 \ (T \geq 60°C) \tag{27}$$

$$T_0 = 60°C \tag{28}$$

5.4 Swelling Pressure

The swelling pressure is calculated using the equation (5) and the coefficient relating to the swelling pressure process F is estimated to be 0.190 based on back analysis using data from laboratory experiment. Figure 5-5 shows the comparison of swelling pressure between measured data and calculated value. F value is obtained at the steady state measured swelling pressure.

5.5 Other Parameter

The specific heat, $(\rho C_v)_m$, and the thermal conductivity, K_{Tm}, of buffer material are given by the function of gravimetric water content, ω, as follows.

$$(\rho C_v)_m = \left(\frac{42.6 + 4.19\omega}{100 + \omega} \right) \left[\frac{kJ}{kg \cdot °C} \right] \tag{29}$$

$$K_{Tm} = (0.050\omega + 0.503) \left[\frac{W}{m \cdot °C} \right] \tag{30}$$

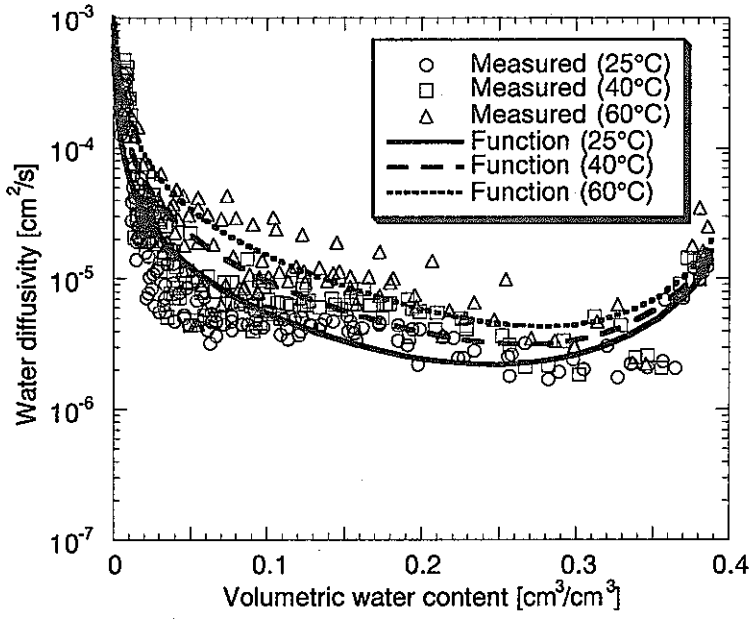

Figure 5-1 Measured and calculated water diffusivity

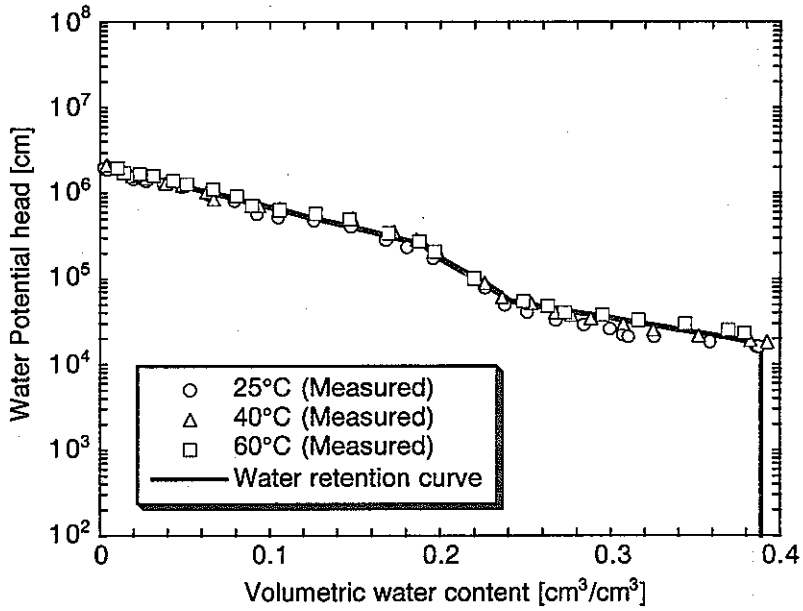

Figure 5-2 Measured and calculated water potential head

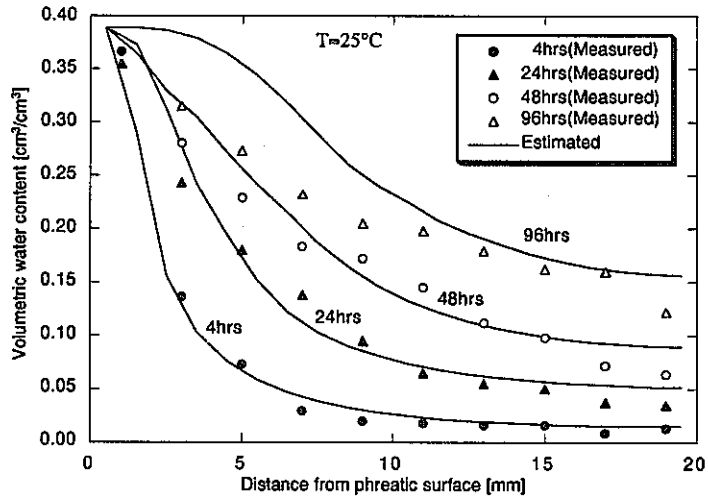

(a) 25°C

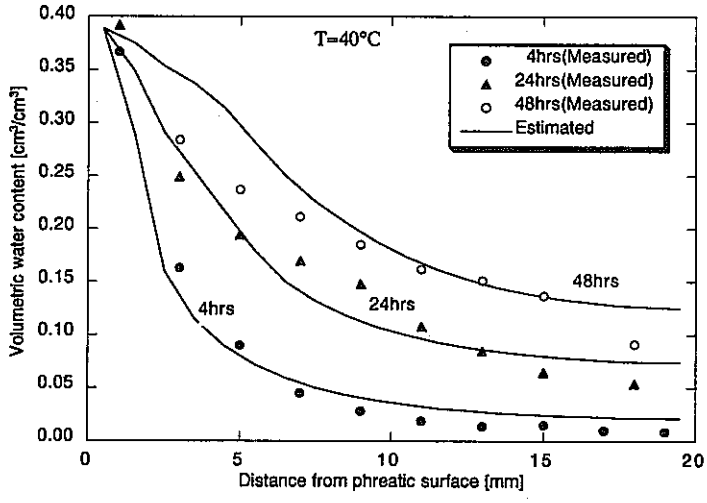

(b) 40°C

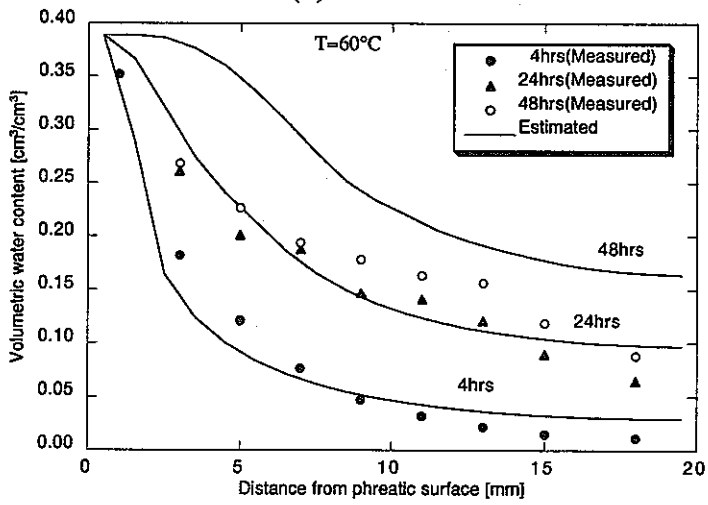

(c) 60°C

Figure 5-3 Comparison between measured and calculated results of water infiltration test under constant temperature condition

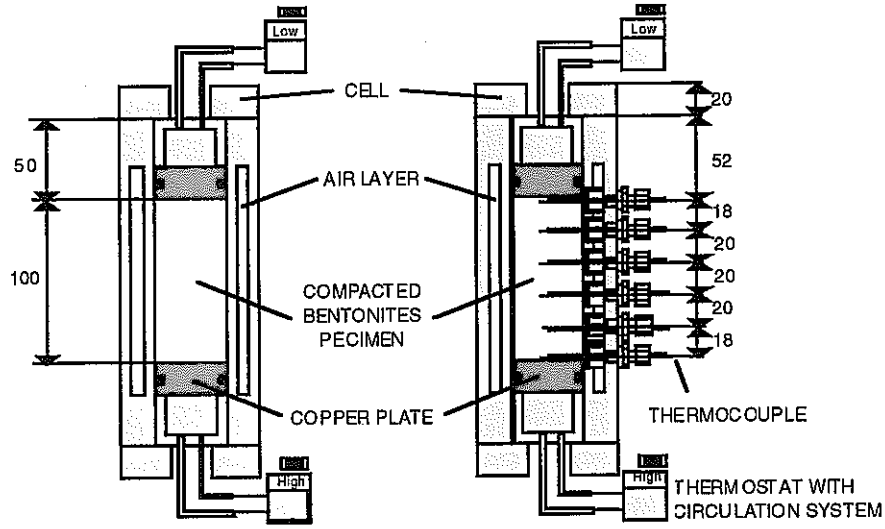

Figure 5-4 Schematic view of KID-BEN equipment

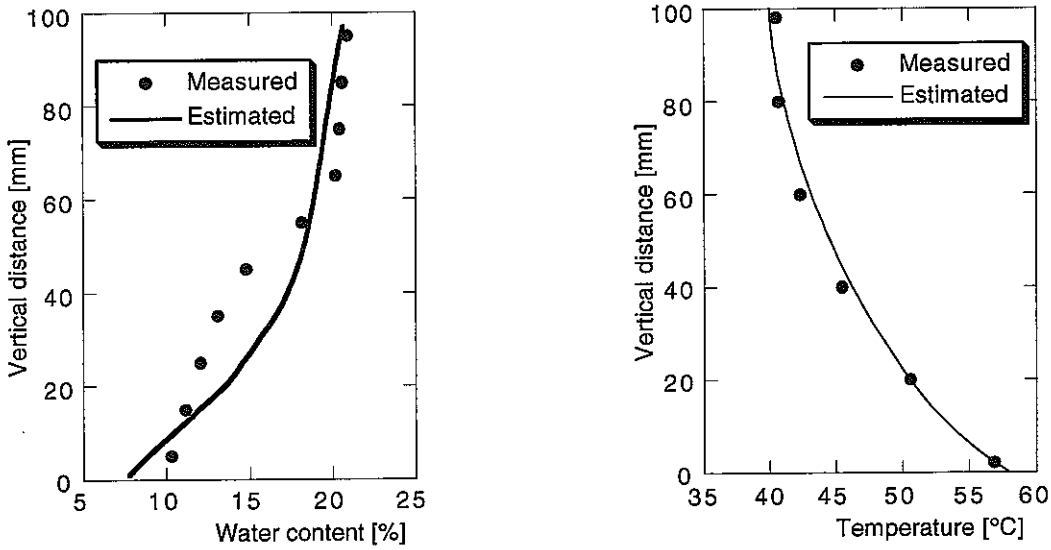

(a) Water content (b) Temperature

Figure 5-5 Comparison between measured and calculated results of water movement test under thermal gradient condition

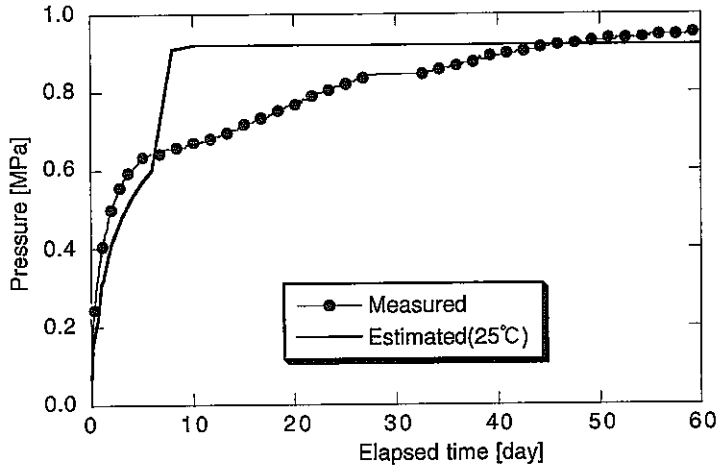

Figure 5-6 Measured and calculated swelling pressure

6. Analysis of Task 2C-1

6.1 Analysis Model

Two dimensional axisymmetric model is used for the analysis of Task 2C-1. The geometry of model is presented in Figure 6-1. The model consists of buffer material, heater, heater guide pipe, steel casing pipe and concrete. The material of heater, heater guide pipe and steel casing pipe is same. The parameters specified in the problem are shown in Table 6-1

The mechanical boundary condition is that all outward boundary surfaces of the model are fixed in the normal direction. The initial temperature is 12.3°C throughout the model. The top boundary of the lid is fixed by the initial temperature. The heat transfer condition is imposed on the other boundaries and the coefficient of heat transfer is 10.0 W/(m^2•°C). The temperature of heater is fix at 100°C.

The two kinds of hydraulic boundary conditions are setting in Task 2C-1 as follows.

(a)zero water flux at all outer boundaries of buffer material(Case 1)

(b)Constant total head at all outer boundaries of buffer material except for the top which has zero water flux (Case 2)

Initial water content of buffer material is 16.5%.

The boundary conditions of two cases are shown in Figure 6-2.

6.2 Results

Figure 6-1 also shows the locations of monitoring points for output specifications of Task 2C-1. The temperature, water content and stress are required.

Figures 6-3 shows the calculated temperature distribution in the buffer material along the Line I of Case 1. Distance expresses that from the center of the model. (a) is before 1 day and (b) is after 1 day. Temperature rises with time until 1 day passage and after that temperature inside the buffer material becomes low. It is considered because of property change of buffer. Figure 6-4 shows the temperature distribution of Case 2. The temperature distribution of Case 2 is almost same with that of Case 1. Figures 6-5 and 6-6 show the time histories of temperature at the output points shown in Figure 6-1. Figure 6-7 shows the temperature distribution map of Case 1 at 250 days passage and Figure 6-8 shows that of Case 2. The temperature distribution of Case 1 is almost same with that of Case 2.

Figure 6-9 shows the calculated water content distribution in the buffer material along the Line I. (a) is a result of Case 1 and (b) is that of Case 2. Water movement of Case 2 is faster than that of Case 1. In Case 2, water content is almost constant after 250 days, while in Case 1, it takes almost 1 year. Furthermore, water content near the heater of Case 1 is lower than that of Case 2. It is because driving force of water movement in Case 1 is only temperature gradient

from the heater to outside. On the other hand, driving force of water movement in Case 2 is temperature gradient from the heater to outside and water supply from the outside. Because of the effect of boundary condition of water flow, the water movement in the buffer is quite different. Figure 6-10 shows the time history of water content, (a) is a result of Case 1 and (b) is that of Case 2. In Case 2, the buffer at the outside part (output points BW1, BW3 and BW6) is saturated instantaneously. Figure 6-11 shows the contour map of degree of saturation of Case 1 at 250 days passage and Figure 6-12 shows that of Case 2.

6.3 Conclusions

This study (Task 2C-1) is to simulate the coupled thermo-hydro-mechanical behavior in the bentonite and to compare the code of each other. The coupled T-H-M process was simulated with fully coupled calculation in our model. From the results, the following conclusions are obtained.

(1) The temperature was not so different with 2 cases. After 1 day from the heating, temperature in the bentonite was maximum in each case and then temperature decrease at the inside of the bentonite.

(2) The water content was almost steady at 250 days passage in Case 2, while it took almost 1 year in Case 1. Furthermore, water content near the heater of Case 1 is lower than that of Case 2. It is because driving force of water movement in Case 1 is only temperature gradient from the heater to outside. On the other hand, driving force of water movement in Case 2 is temperature gradient from the heater to outside and water supply from the outside.

Table 6-1 Parameters of materials for analysis

Parameter	Concrete	Buffer	Heater
Young's modulus [MPa]	$2.5 \bullet 10^{4}$	$2.5 \bullet 10^{2}$	$2.0 \bullet 10^{5}$
Poisson's ratio [-]	0.167	0.3	0.3
Density [g/cm^3]	2.3	1.87	7.8
Hydraulic conductivity [cm/s]	$1.0 \bullet 10^{-12}$	$2.0 \bullet 10^{-11}$	$1.0 \bullet 10^{-18}$
Specific heat [kJ/kg °C]	0.75	Eq.(29)	0.46
Thermal conductivity [W/m °C]	1.88	Eq.(30)	53.0
Thermal expansion [1/°C]	$1.0 \bullet 10^{-6}$	$1.0 \bullet 10^{-6}$	$1.64 \bullet 10^{-6}$

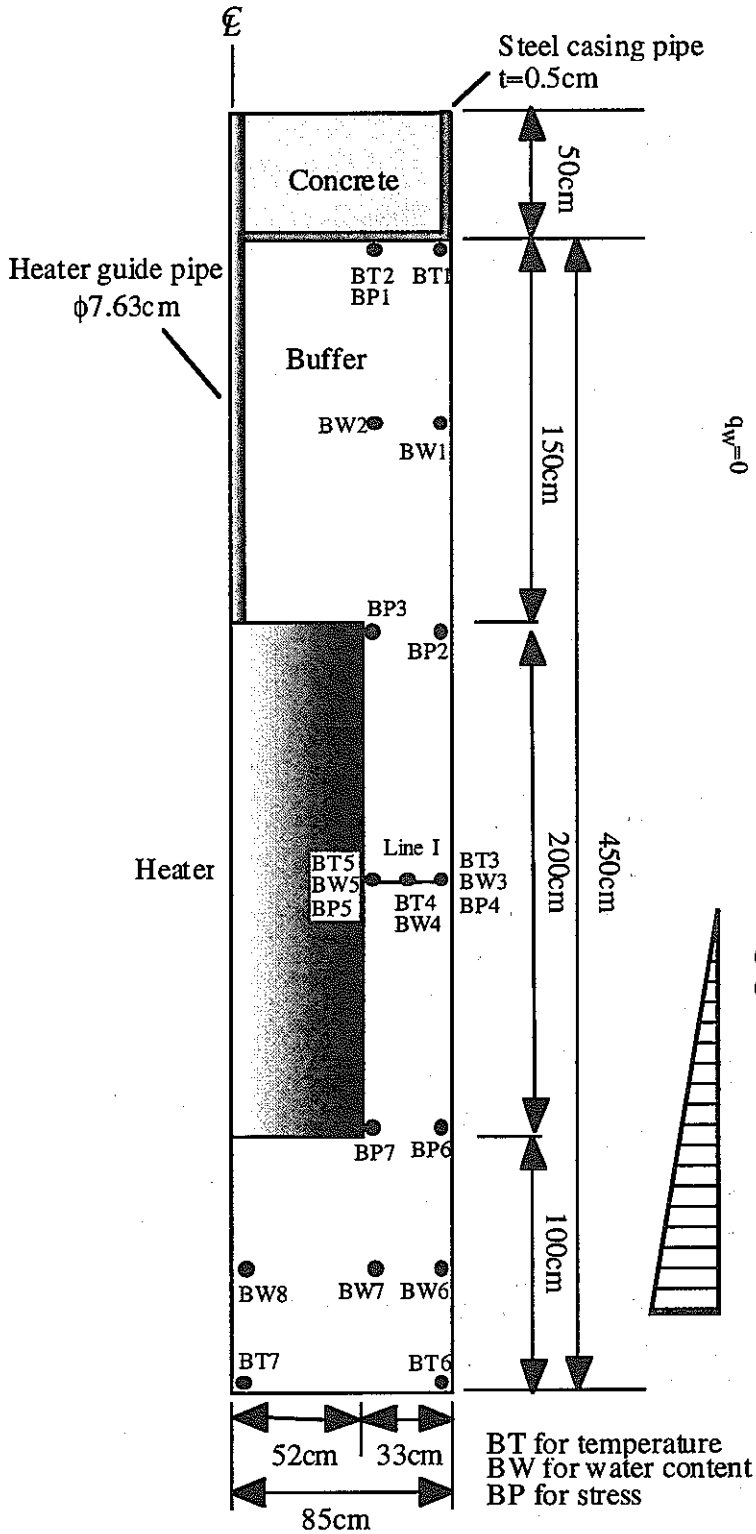

Figure 6-1 Model geometry

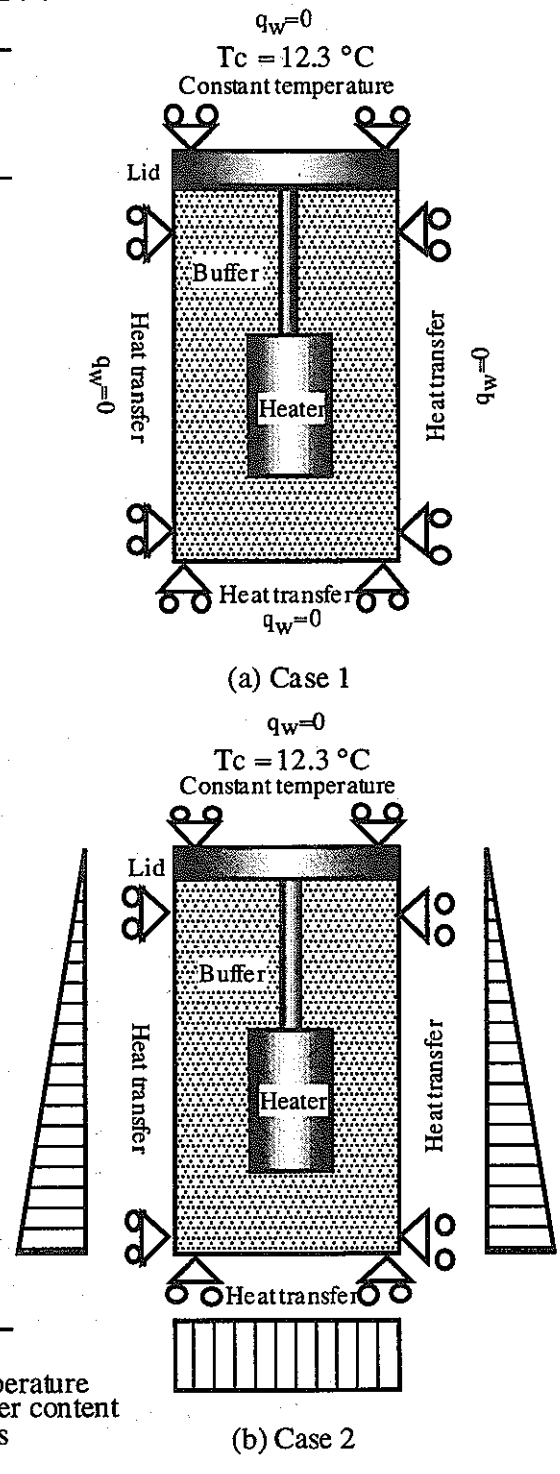

Figure 6-2 Boundary conditions

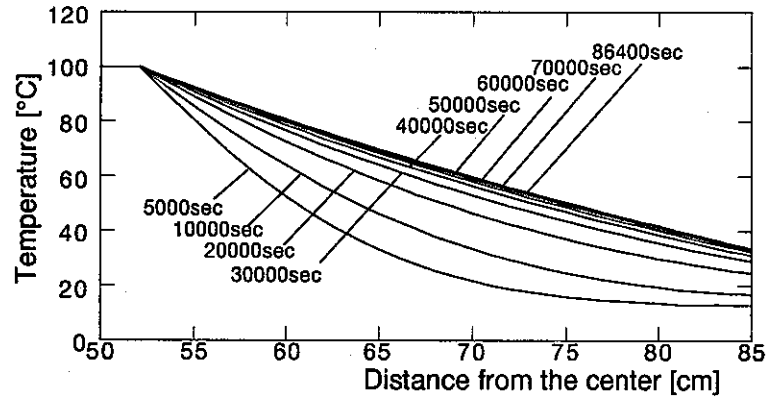

(a) After 5000 sec to 1 day

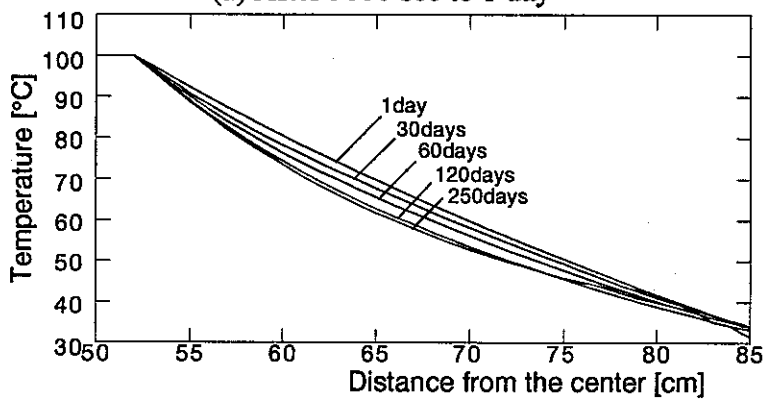

(b) After 1 day to 250 days

Figure 6-3 Temperature distribution along the Line I (Case 1)

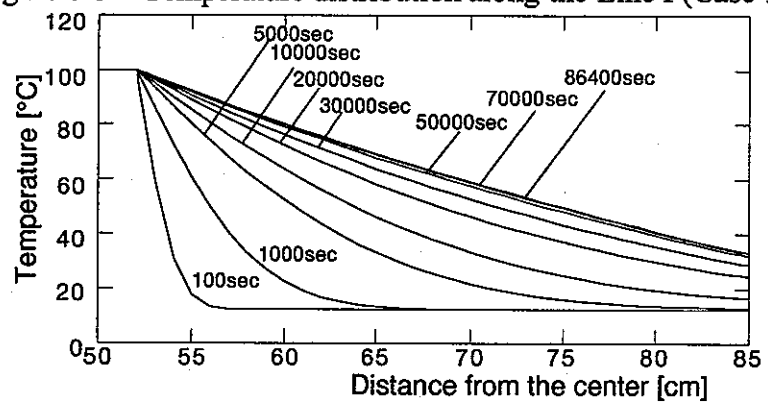

(a) After 5000 sec to 1 day

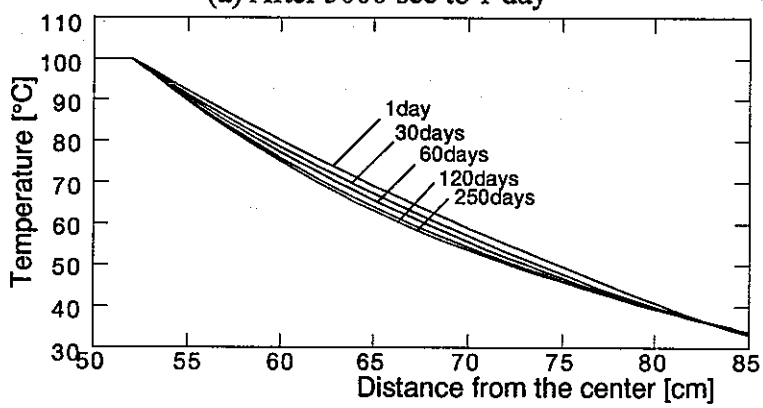

(b) After 1 day to 250 days

Figure 6-4 Temperature distribution along the Line I (Case 2)

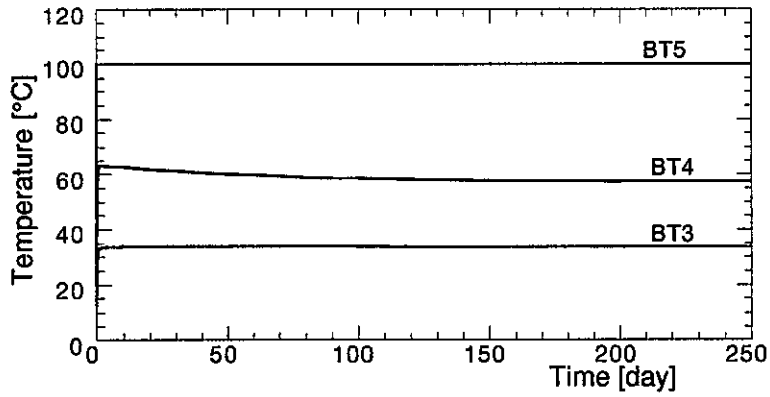

(a) Output points BT3, BT4 and BT5

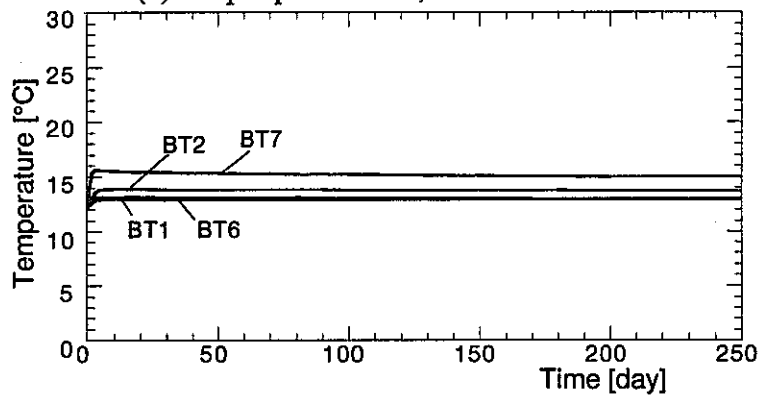

(b) Output points BT1, BT2, BT6 and BT7

Figure 6-5 Time history of temperature in the buffer (Case 1)

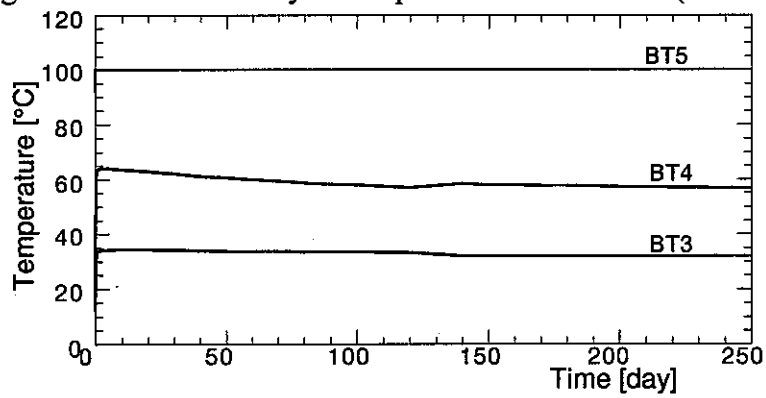

(a) Output points BT3, BT4 and BT5

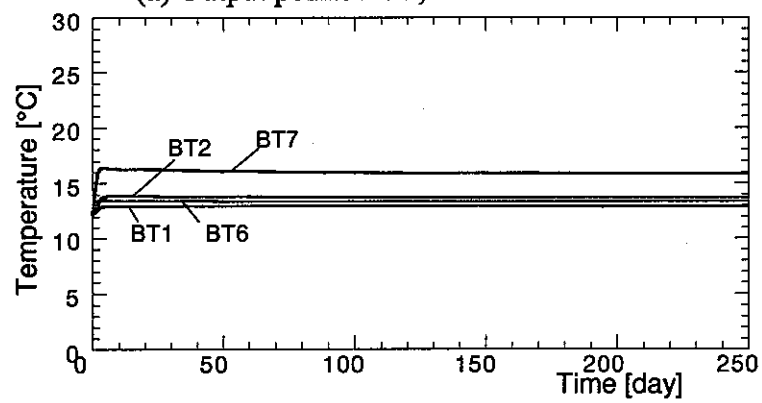

(b) Output points BT1, BT2, BT6 and BT7

Figure 6-6 Time history of temperature in the buffer (Case 1)

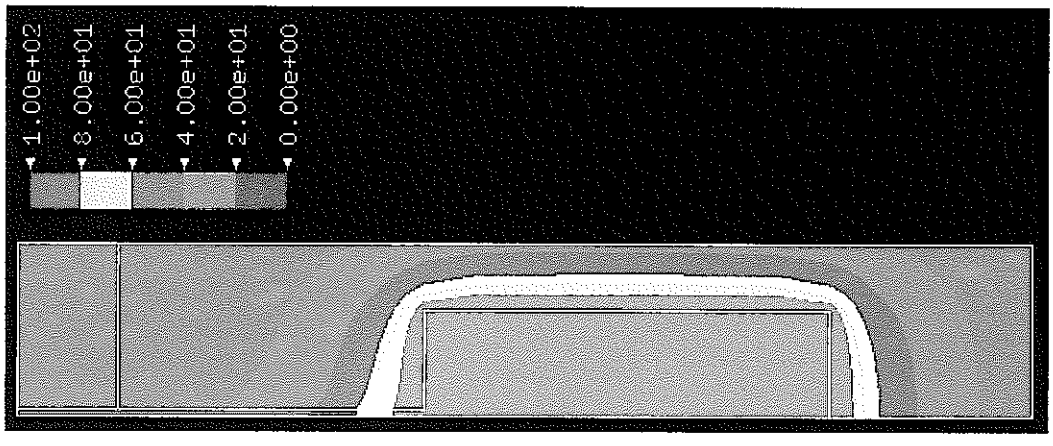

(a) After 1 day

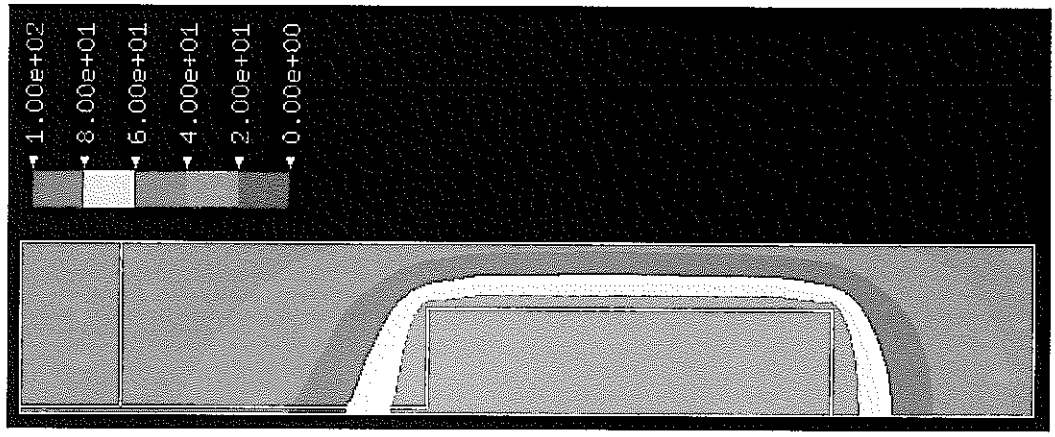

(b) After 30 days

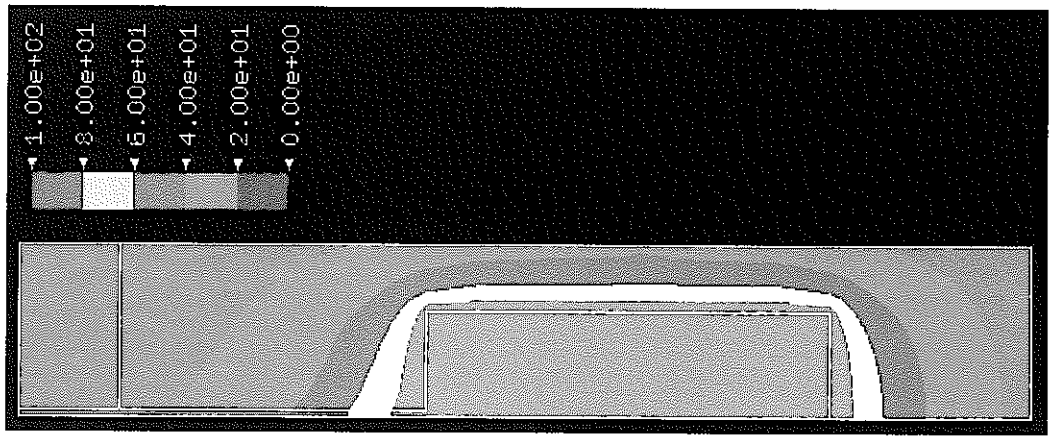

(c) After 250 days

Figure 6-7 Contour of temperature (Case 1)

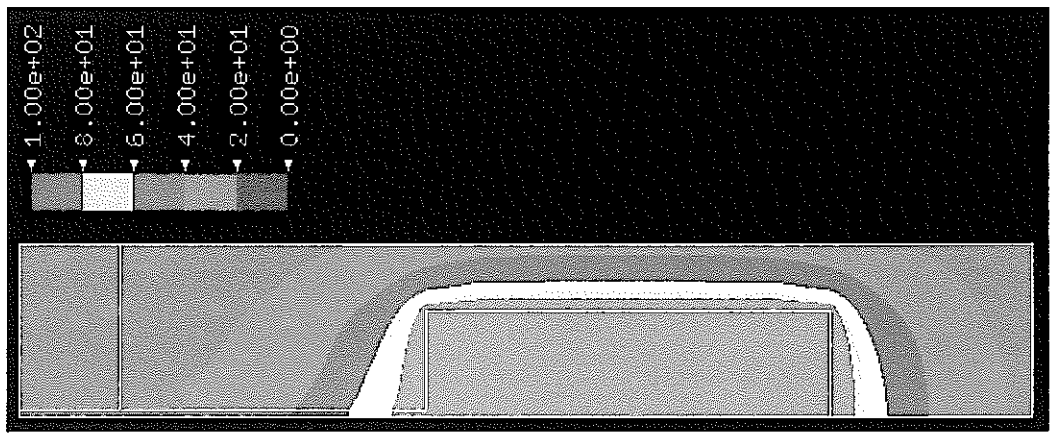

(c) After 250 days

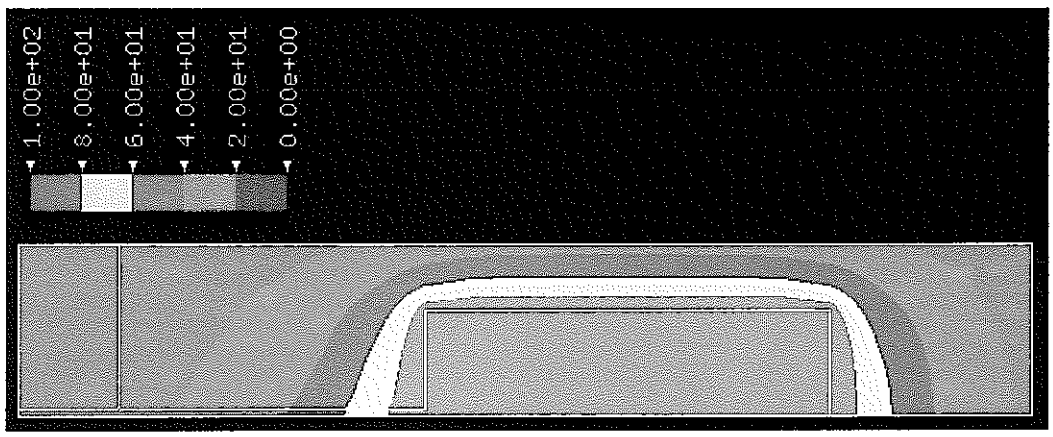

(b) After 30 days

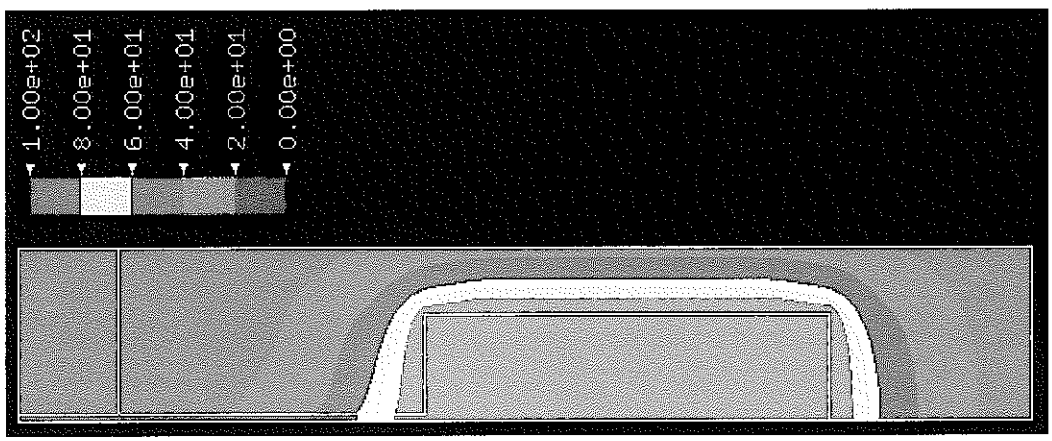

(a) After 1 day

Figure 6-8 Contour of temperature (Case 2)

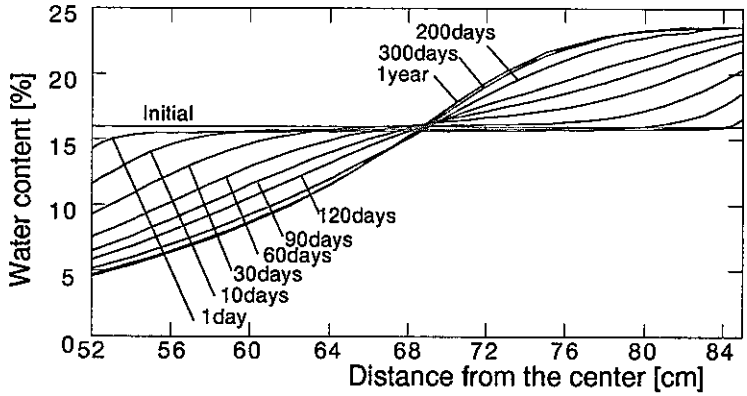

(a) Case 1

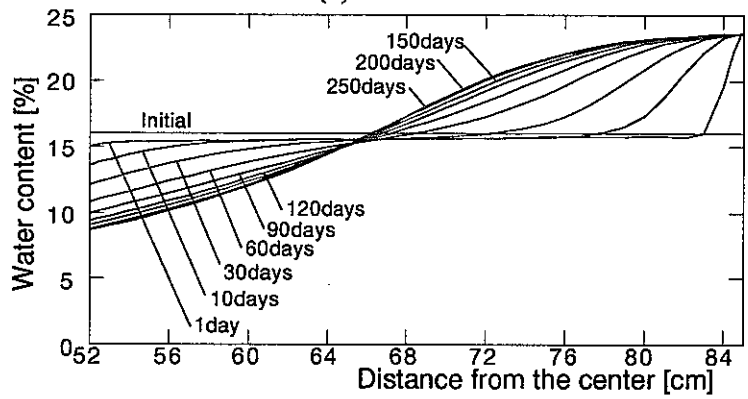

(b) Case 2

Figure 6-9 Water content distribution along the Line I

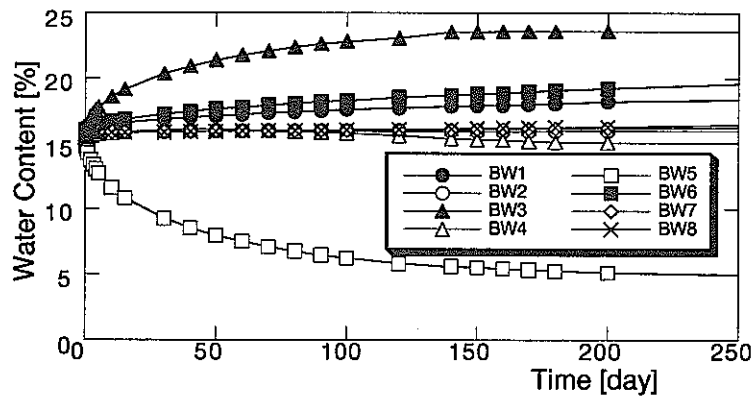

(a) Case 1

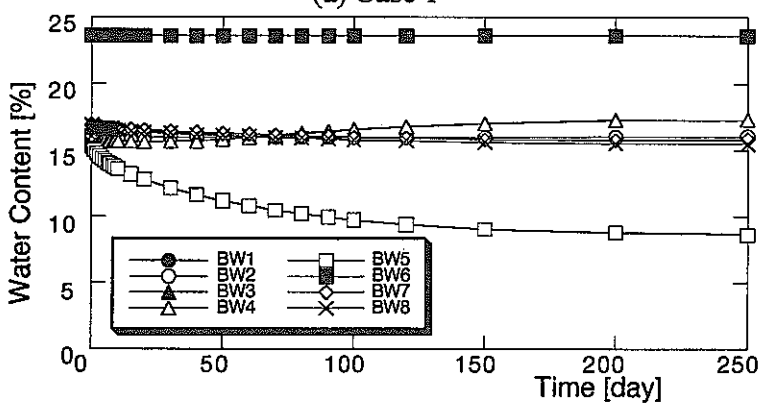

(b) Case 2

Figure 6-10 Time history of water content in the buffer

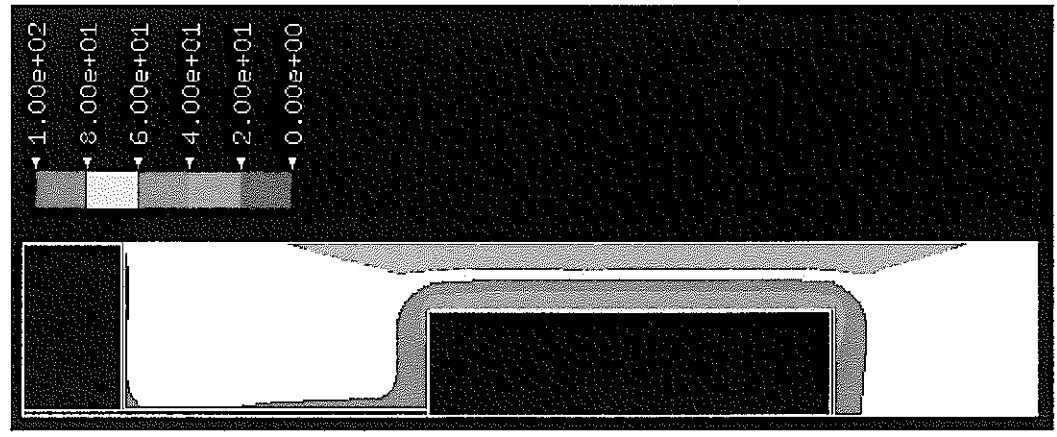

(c) After 250 days

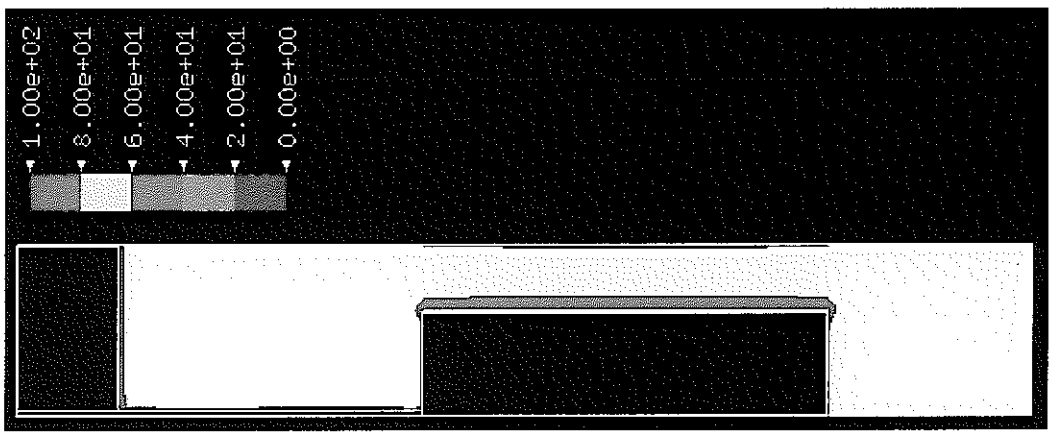

(b) After 30 days

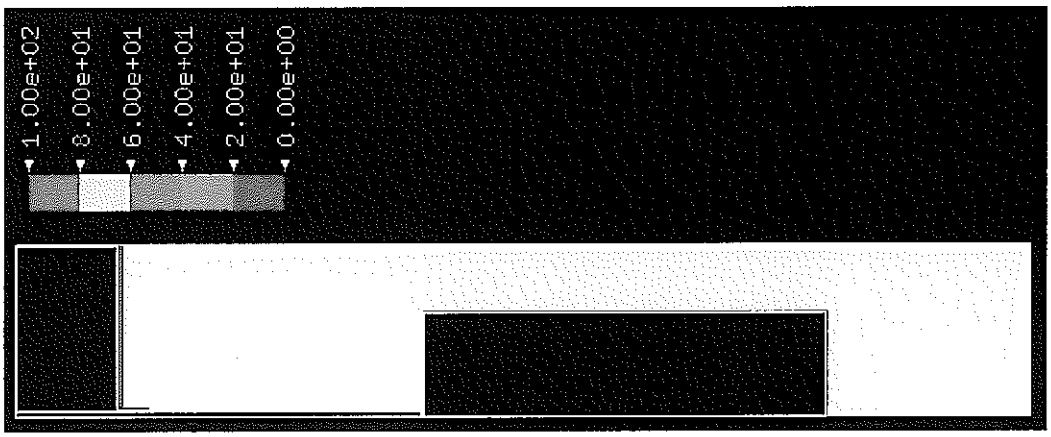

(a) After 1 day

Figure 6-11 Contour of degree of saturation in the buffer (Case 1)

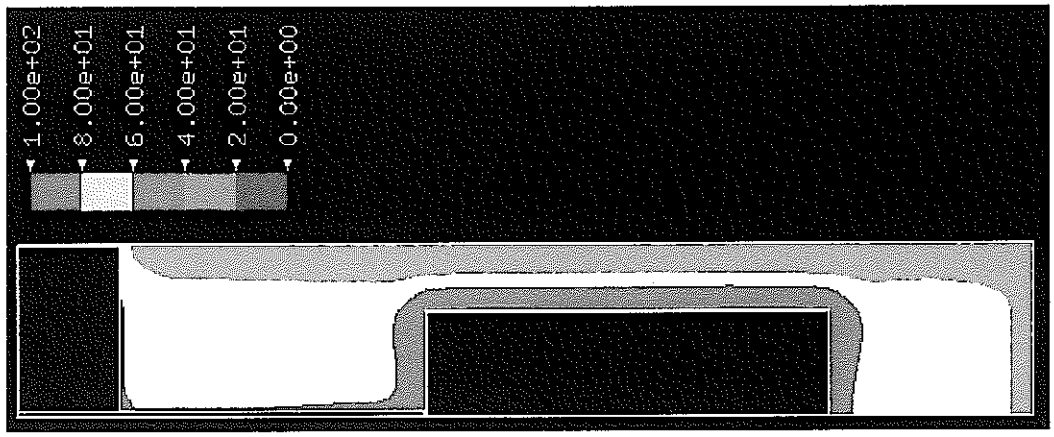

(c) After 250 days

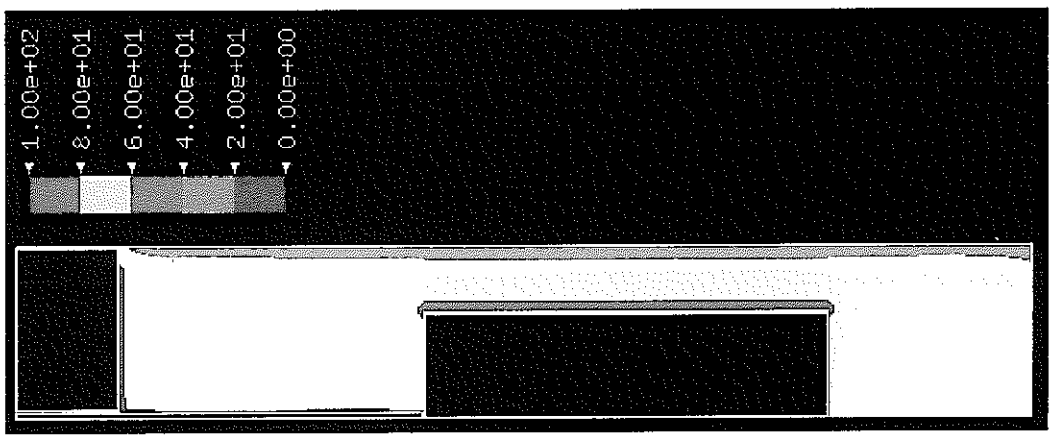

(b) After 30 days

(a) After 1 day

Figure 6-12 Contour of degree of saturation in the buffer (Case 2)

7. Analyses of Task 2C-2

7.1 Analysis Model

Two dimensional axisymmetric model is used for the analysis of Task 2C-2 in this section. The objective of this section is to estimate the T-H-M phenomena in the buffer and to confirm the effect of permeability of rock mass upon T-H-M phenomena in the buffer. The geometry of model is presented in Figure 7-1. The model consists of rock mass, buffer material, heater and steel lid. In analysis of Task 2C-1, heater guide pipe, steel casing pipe and concrete are considered in the model. However, the effect of heater guide pip and concrete is small. Therefore, only steel lid is considered in this section. The material of heater and steel lid is same.

The mechanical boundary condition is that all outward boundary surfaces of the model are fixed in the normal direction. The initial temperature is 12.3°C throughout the model. The outer boundary of the model is fixed at the initial temperature. The temperature of heater is fix at 100°C. Initial water content of buffer material is 15.0 % and rock mass has hydrostatic water pressure at the flooding pool condition of 40 cm on the floor of the test drift. The outer boundary of model is constant at the initial water head. The boundary conditions are also shown in Figure 7-1.

The unsaturated property of rock mass is assumed as Figure 7-2. This property was estimated by Prof. Watanabe. [Watanabe, K., 1991] The other parameters specified in the problem are shown in Table 7-1.

Table 7-1 Parameters of materials for analysis

Parameter	Heater and Lid	Buffer	Rock
Young's modulus [MPa]	$2.0 \bullet 10^{5}$	$2.5 \bullet 10^{2}$	$2.81 \bullet 10^{4}$
Poisson's ratio [-]	0.3	0.3	0.3
Density [g/cm^3]	7.8	1.87	2.75
Hydraulic conductivity [cm/s]	$1.0 \bullet 10^{-18}$	$2.0 \bullet 10^{-11}$	$1.98 \bullet 10^{-7}$
Specific heat [kJ/kg °C]	0.46	Eq.(29)	0.833
Thermal conductivity [W/m °C]	53.0	Eq.(30)	2.7
Thermal expansion [1/°C]	$1.64 \bullet 10^{-6}$	$1.0 \bullet 10^{-6}$	$1.0 \bullet 10^{-6}$

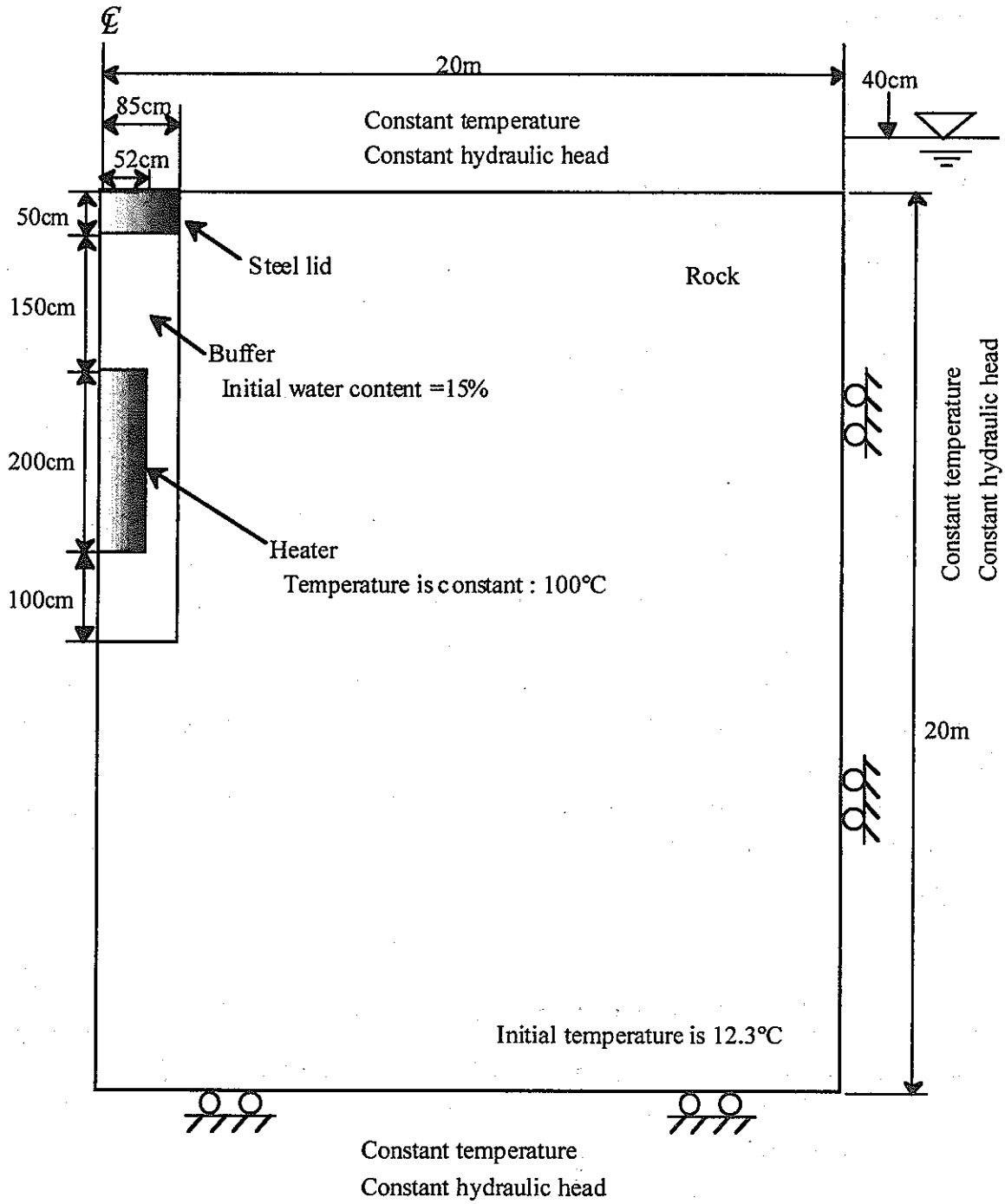

Figure 7-1 Model geometry and boundary conditions

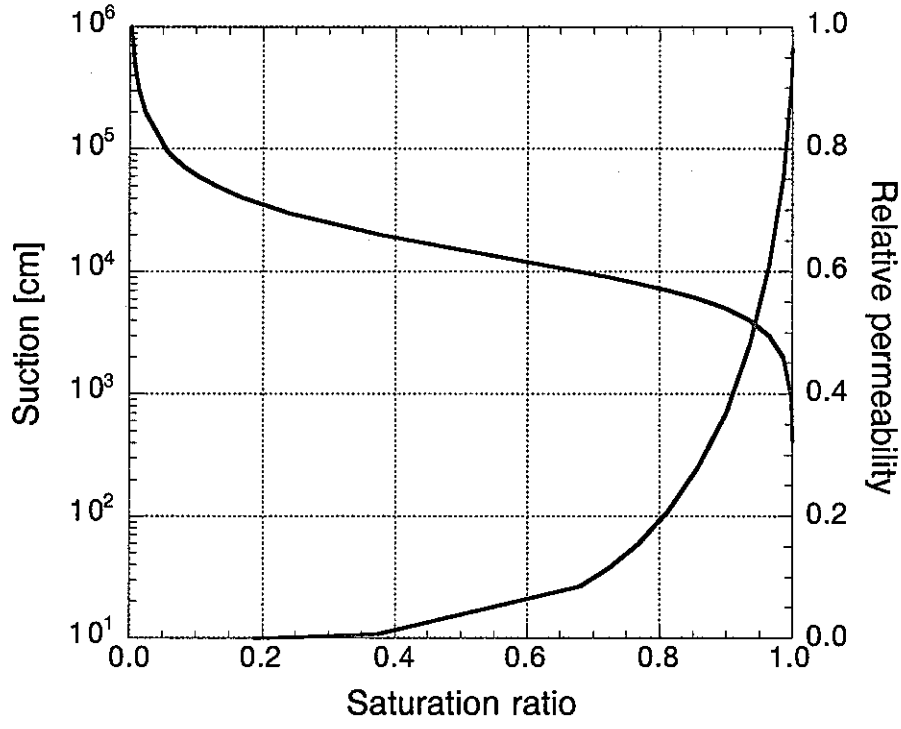

Figure 7-2 Unsaturated property of rock mass

7.2 Analysis results (Heating phase)

Figure 7-3 shows the locations of output points and line. Output points in the buffer are same with those of Task 2C-1. In the rock mass output points are along the boreholes KBH5 and KBH6. The sensors were set at the same points with output points.

Figure 7-4 shows the calculated temperature distribution along the output line. Distance expresses that from the center of the model. Temperature becomes constant after 5 months from the start of heating. Figure 7-5 shows the calculated water content distribution along the output line. Water content near the heater becomes low due to temperature gradient and water content near the rock mass becomes high, then water content does not become constant after 255 days. Figure 7-6 shows the distribution of temperature in the model. Figure 7-6 (a) shows temperature distribution at 1 month passage from the start of heating and (b) shows that at the 8 months passage. The temperature spreads homogeneously and becomes constant at 1 month passage. Figure 7-7 shows the distribution of water content in the buffer. Figure 7-7 (a) shows temperature distribution at 1 month passage from the start of heating and (b) shows that at the 8 months passage. The buffer around the heater is drying and that near the rock mass is wetting. Figure 7-8 shows the time histories of temperature at the output points in the rock mass and Figure 7-9 shows those in the buffer material. The temperature in the buffer

becomes constant at the 30 days passage, while it takes 150 days in the rock mass. Figure 7-10 shows the time histories of water content at the output points in the buffer material. Outside part of buffer is saturated immediately, while inside part of buffer dries in time. After 250 days from the start of heating, water content near the heater becomes about 2.0 %. Figure 7-11 shows the time histories of water pressure in the rock mass. The water pressure near the buffer mass becomes negative value right after the heating and then it increases as time passage. At first water pressure becomes negative but rock mass is saturated, because capillary pressure of the rock is high as shown in Figure 7-2. Figure 7-12 shows the time histories of the total pressure. The total pressure increases gradually and total pressure at the outer part is higher than that at the inner part. The total pressure is not constant at 250 days passage. Figure 7-13 shows the change of the void ratio in the buffer. The void ratio decrease gradually and change at the outer part is higher than that at the inner part.

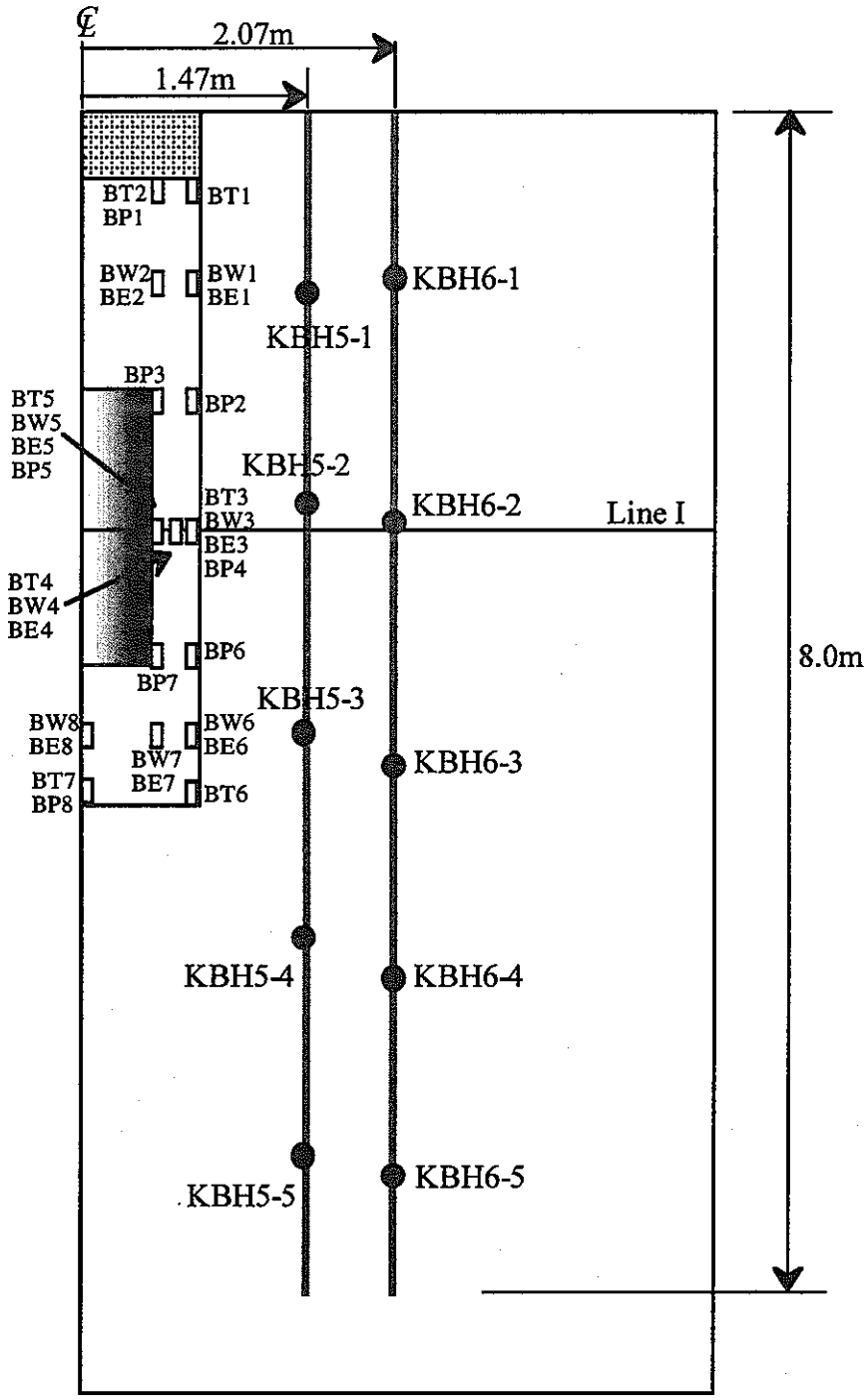

Figure 7-3 Output points and line

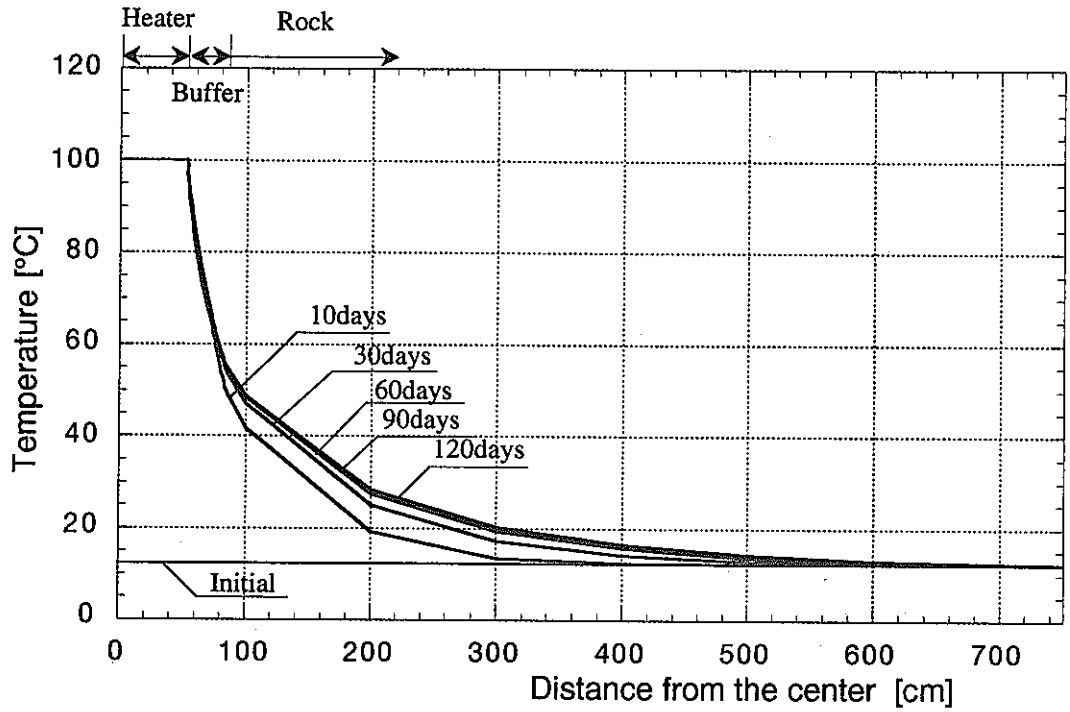

Figure 7-4 Temperature distribution along the Line I (Heating phase)

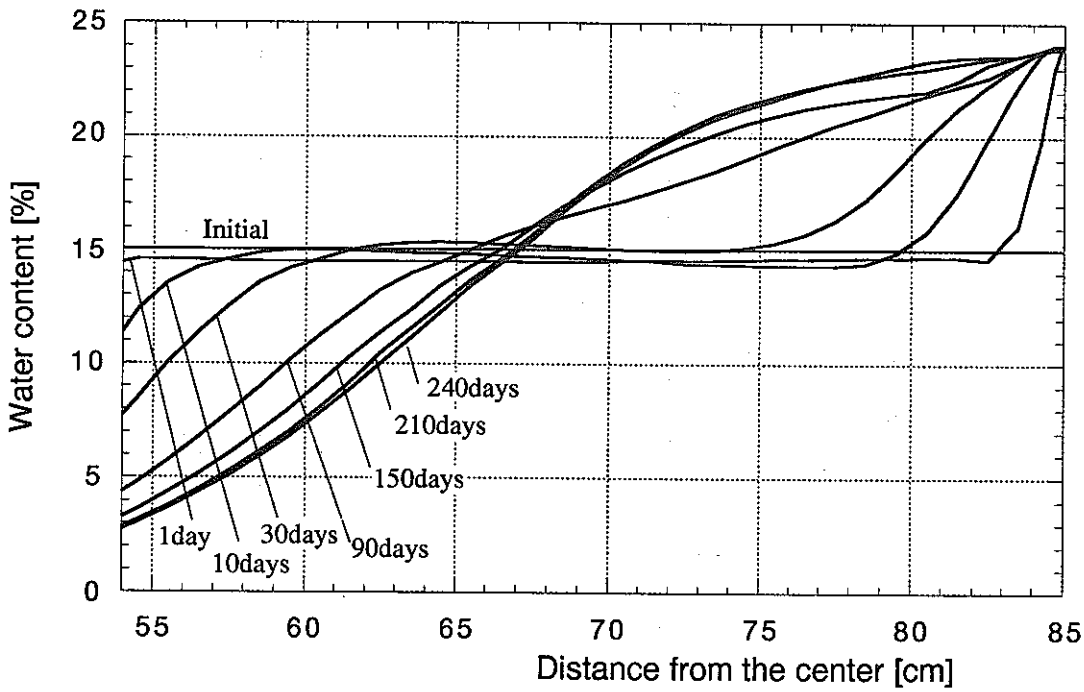

Figure 7-5 Water content distribution along the Line I (Heating phase)

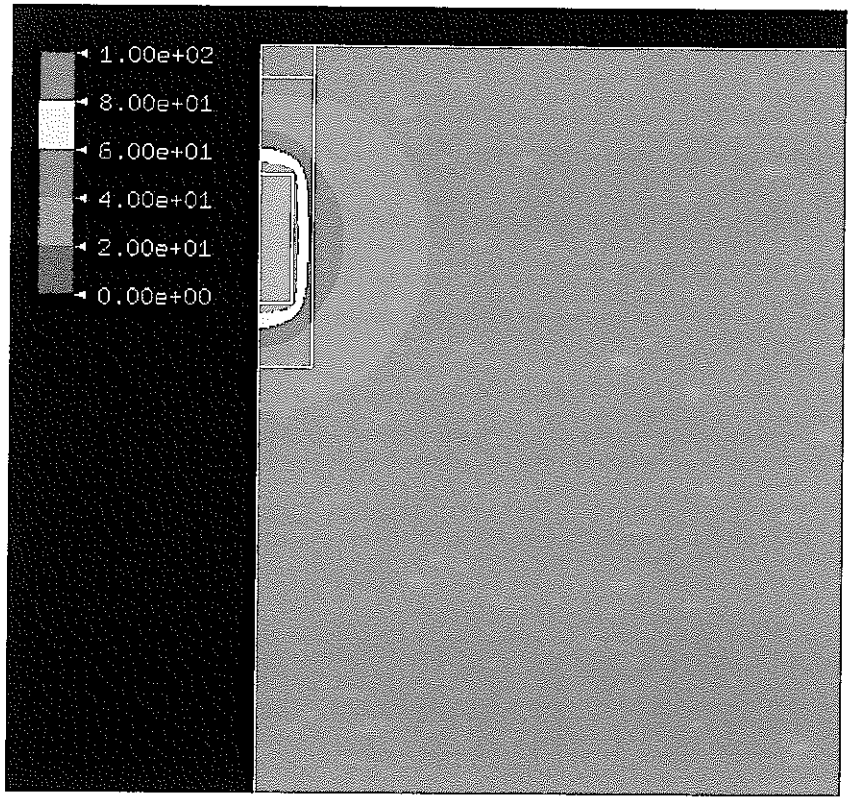

(a) After 1 month

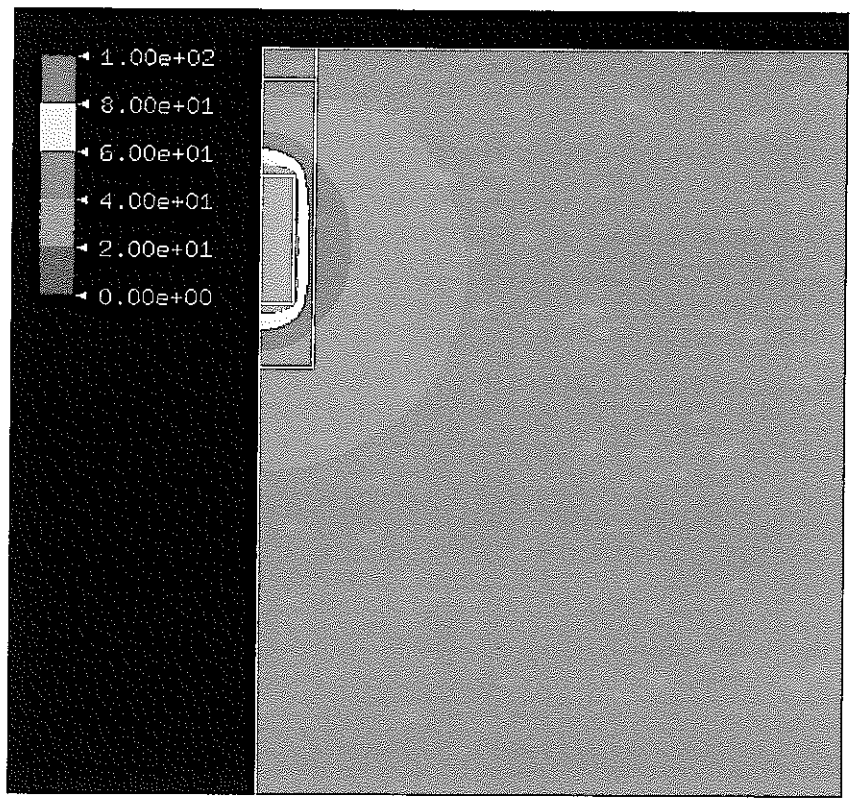

(b) After 8 months

Figure 7-6 Temperature distribution around the test pit

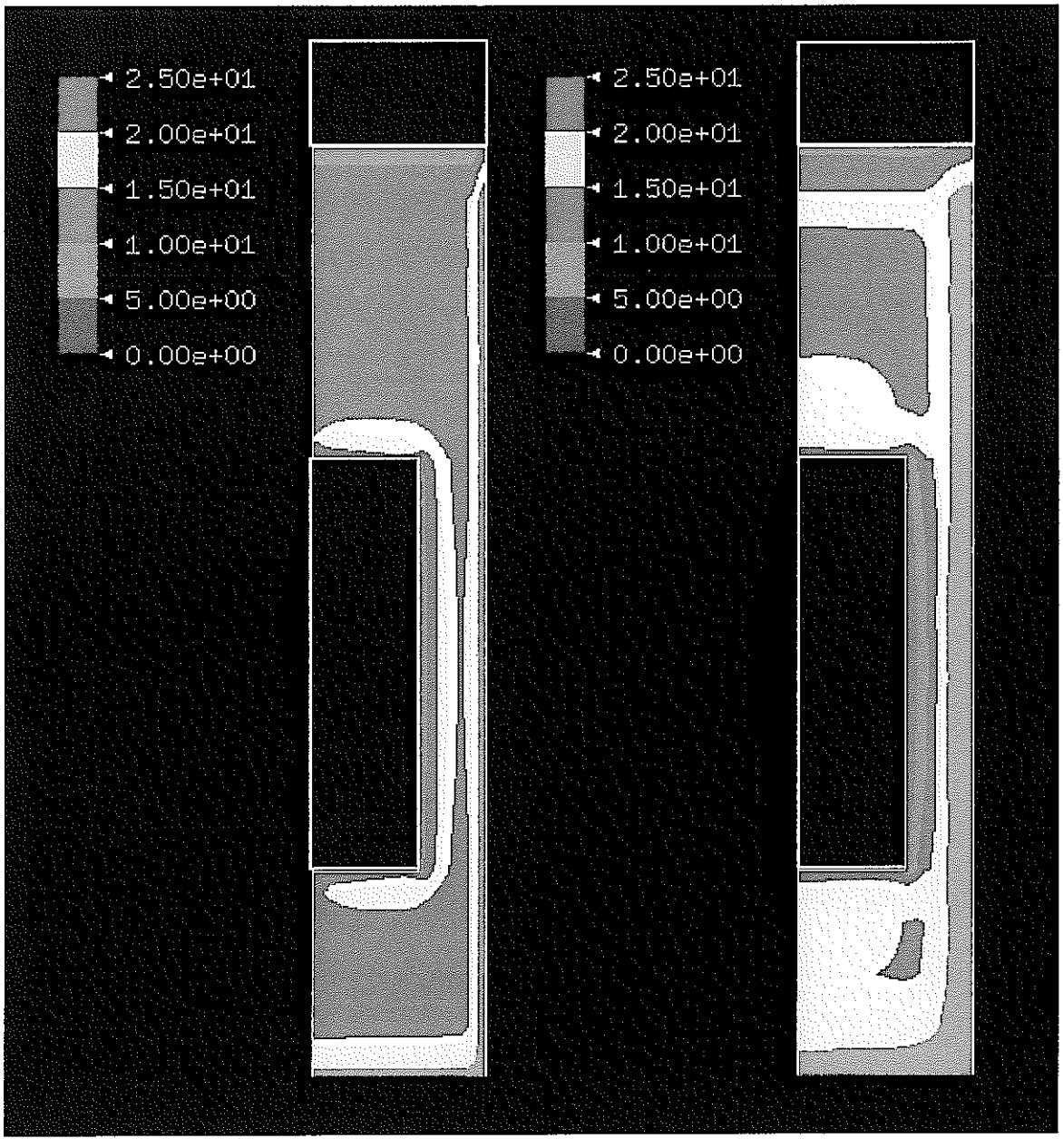

(a) After 1 month (b) After 8 months

Figure 7-7 Water content distribution in the buffer

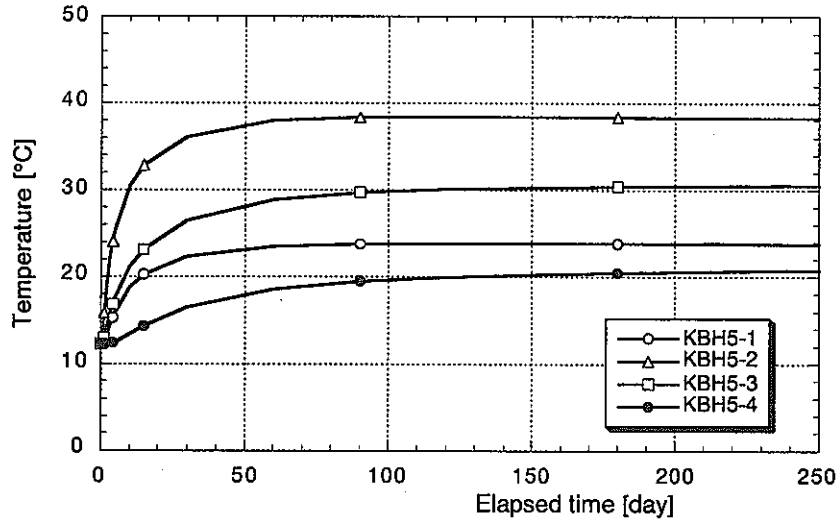

(a) KBH5

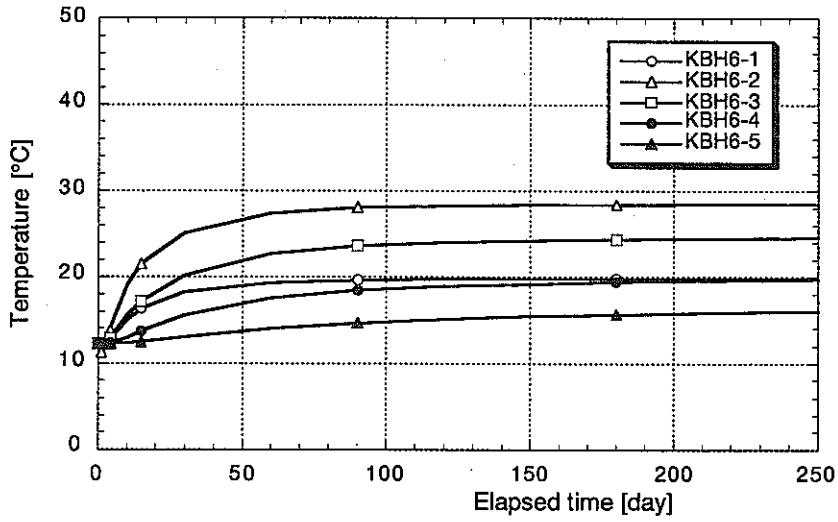

(b) KBH6

Figure 7-8 Time history of temperature in the rock mass

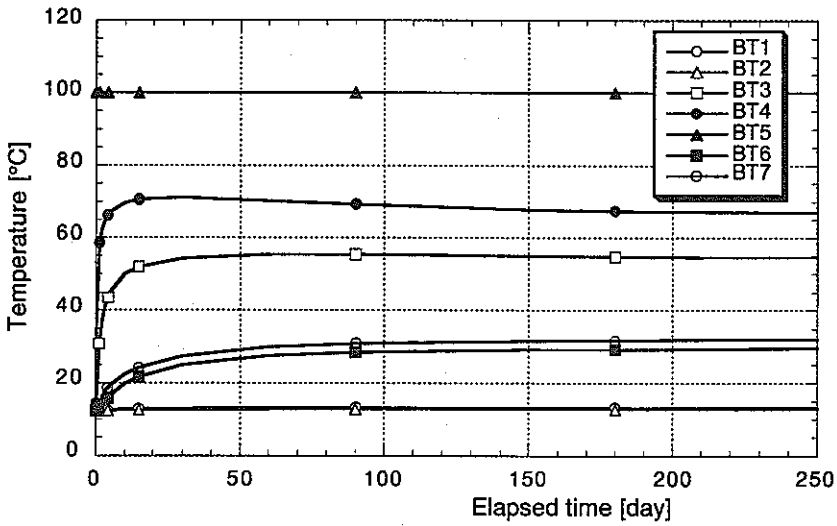

Figure 7-9 Time history of temperature in the buffer

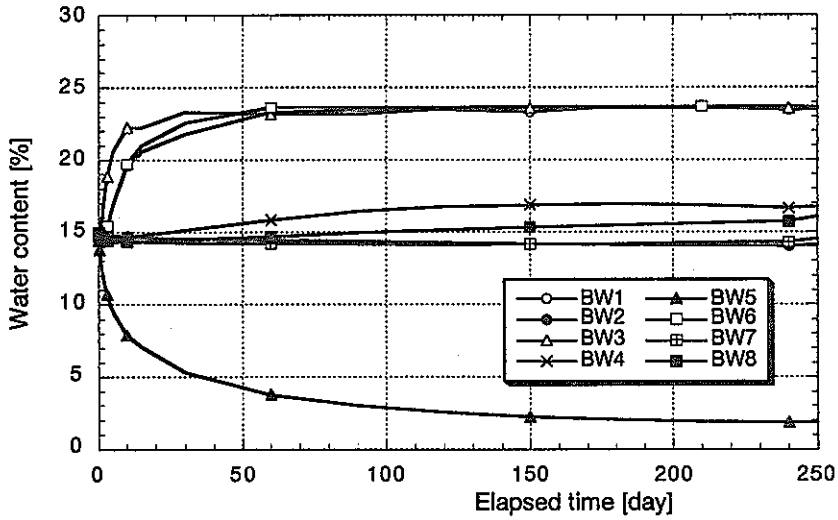

Figure 7-10 Time history of water content in the buffer

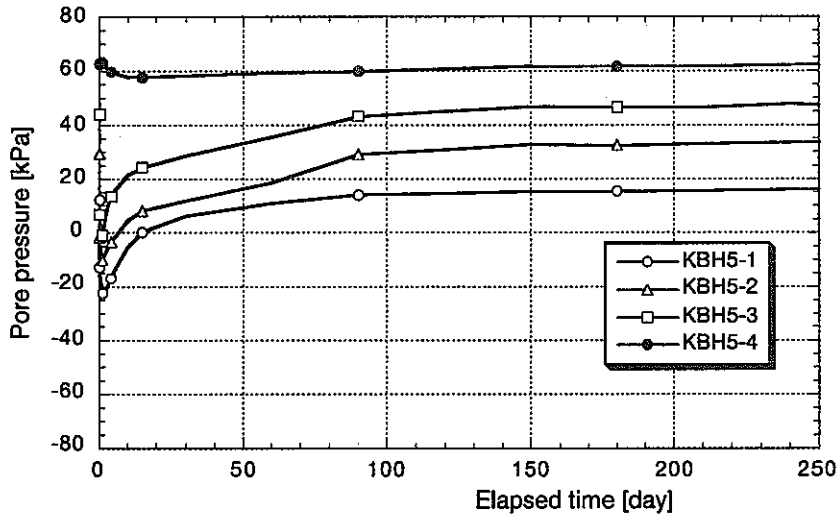

(a) KBH5

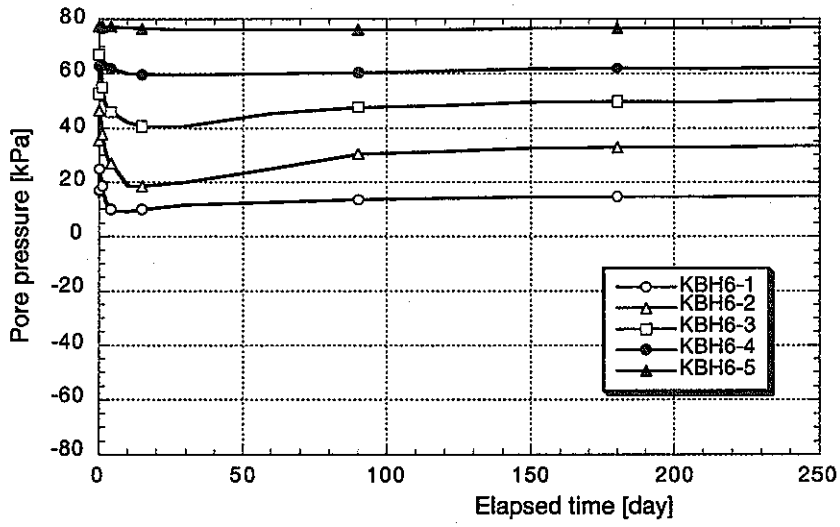

(b) KBH6

Figure 7-11 Time history of pore pressure in the rock mass

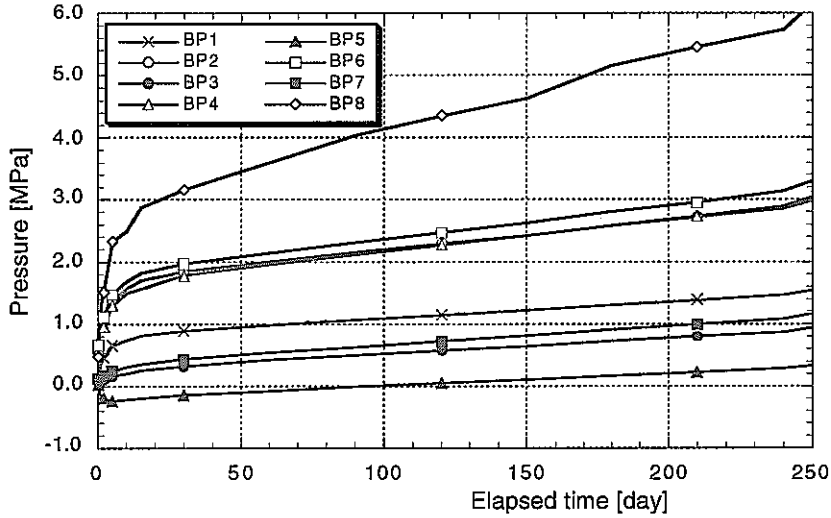

Figure 7-12 Time history of stress in the buffer

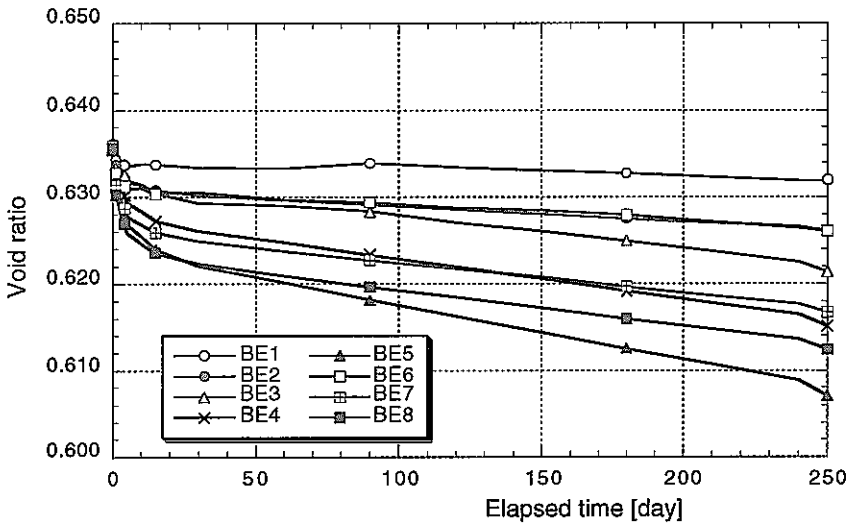

Figure 7-13 Time history of void ratio in the buffer

7.3 Comparison between the measured and calculated results (Heating phase)

Figures 7-14, 7-15, 7-16 and 7-17 show the comparison between the measured and calculated results. Figure 7-14 shows the comparison of temperature in the rock mass, (a) is at the borehole KBH5 and (b) is at the borehole KBH6. Figure 7-15 shows the comparison of temperature in the buffer, (a) is at the upper and lower part of buffer, (b) is at the center level of buffer. Figure 7-16 shows the comparison of water content in the buffer. Figure 7-17 shows the comparison of water content distribution at the end of heating phase. Measured data were obtained by sampling and laboratory test at the 250 days passage from the start of heating.

A tendency of temperature rise of calculated results is almost same with measured one but final values of calculated results are a little high except for the center level of buffer material. A tendency of water content change of calculated results is similar to the measured results. However, the speed of water movement of calculated results is a little higher that that of measured results. Furthermore, the measured water content at the point of 15 cm apart from the heater (middle part) is raised at first and then goes down. It is considered that water in the buffer at the middle part is wetting at first, and as time passed, the buffer at the same part is drying because water moves to outside further. This phenomenon can not be simulated in this analysis. The calculated water movement is smoother than that of measured one. The water content distribution along GL -300 cm level is almost same between measured and calculated results. As a whole, calculated water content around the heater is good agreement with measured values. While, calculated water content near rock mass is higher than measured data. It is considered that the reason of this discrepancy is due to use of inappropriate property of thermal water diffusivity or hydraulic property of rock mass and so on.

Figure 7-18 shows the comparison of total pressure in the buffer mass. The total pressure at the outside part (near rock mass) of buffer was not measured [Chijimatsu, M., et al, 1999]. The reason is considered that the pressure cell that was used in this test is small, so, it did not work well because of roughness of rock surface. Therefore, comparison of total pressure is conducted about inside part (near heater) of buffer. Measured values are between 0kPa and 500kPa, and become almost steady state at the early period. On the other hand, calculated values become negative just after the start of heating and increase gradually because of the effect of swelling pressure at the center level of heater (BP5). The use of unsuitable thermal expansion value of buffer material is considered to be the one cause of this discrepancy. The calculated total pressure at the upper part and lower part of heater increase gradually from the start of heating. And it does not become steady state at the end of heating phase.

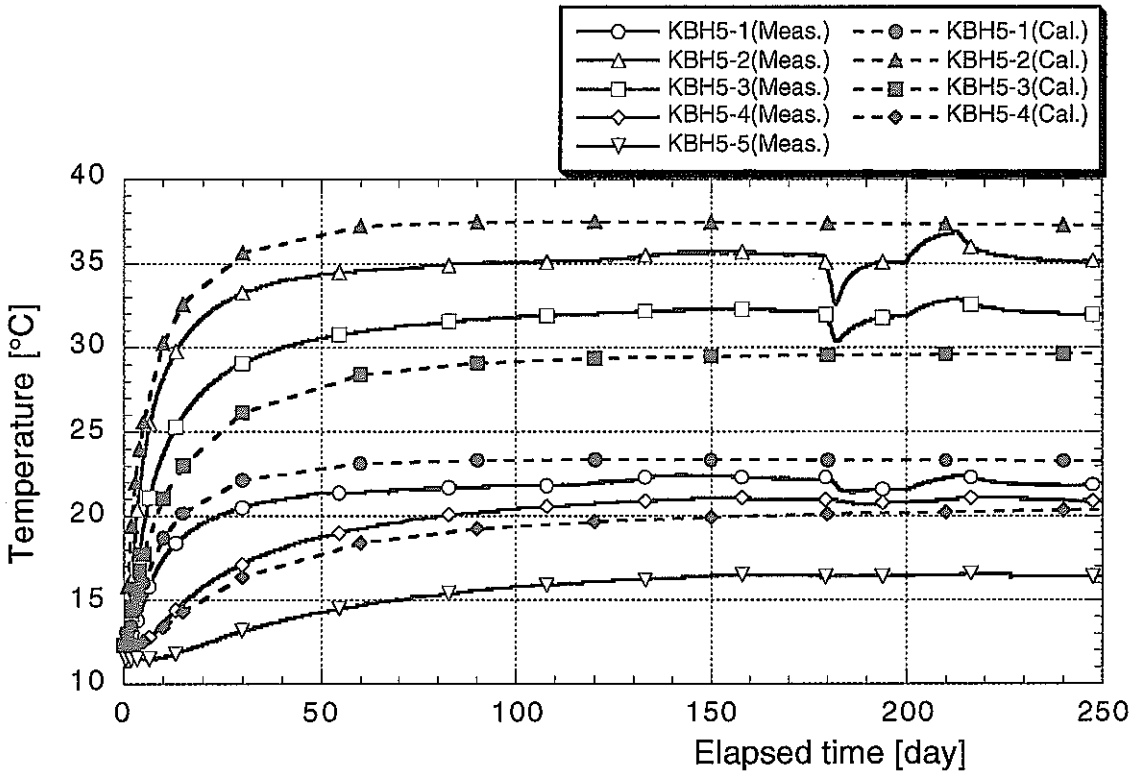

(a) KBH5

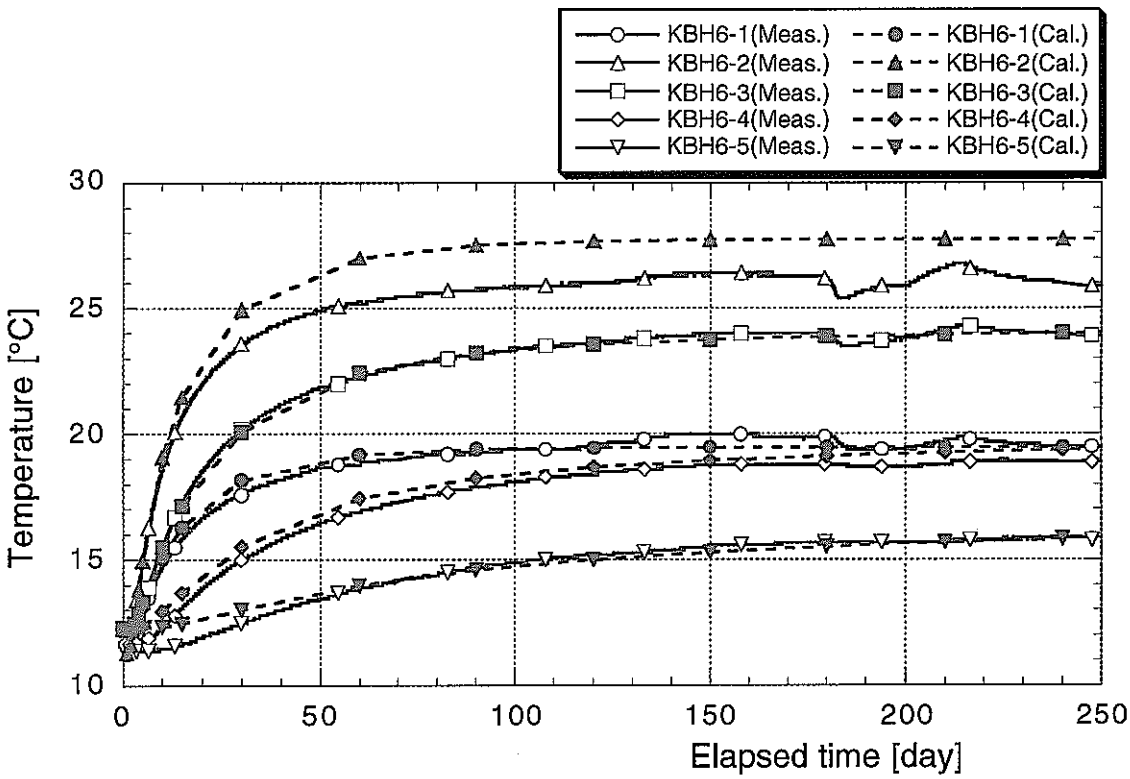

(b) KBH6

Figure 7-14 Comparison of the temperature in the rock mass (Heating phase)

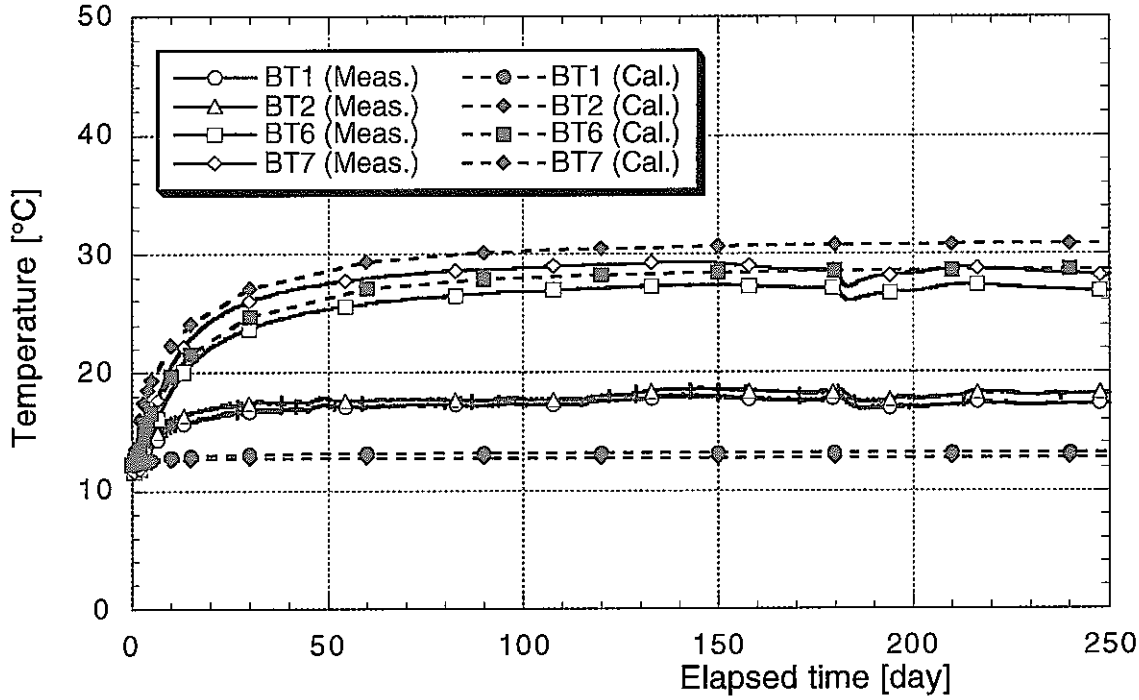

(a) Upper and Lower part of the buffer

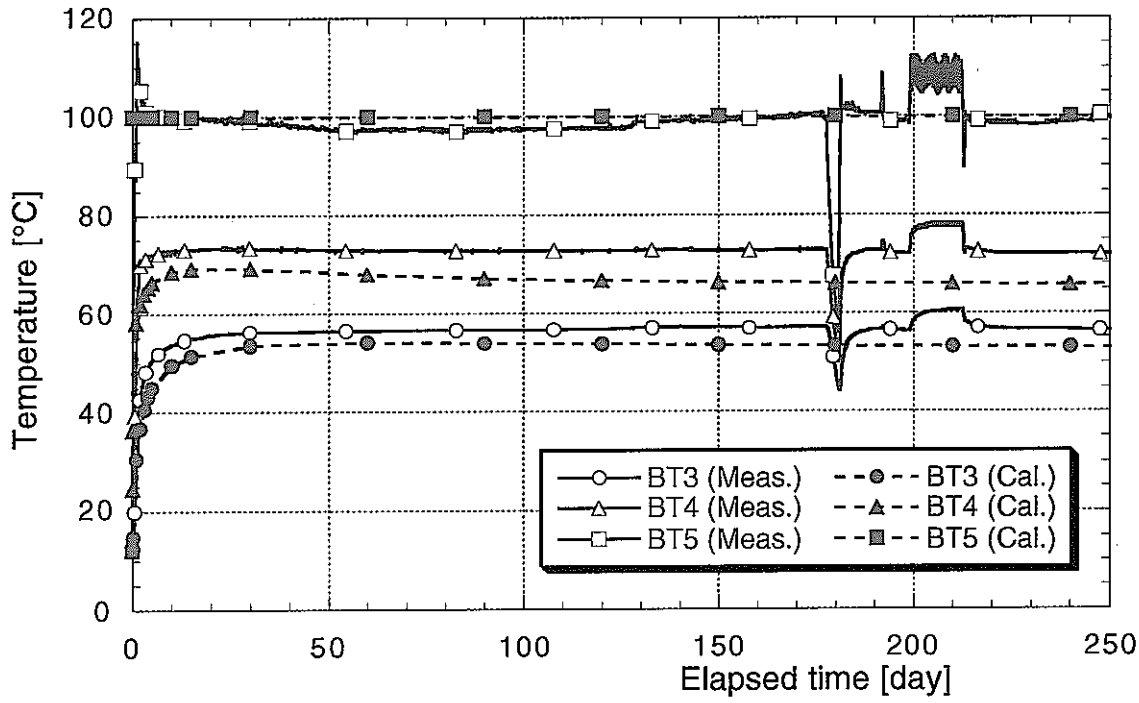

(b) Center level of the buffer

Figure 7-15 Comparison of temperature in the buffer

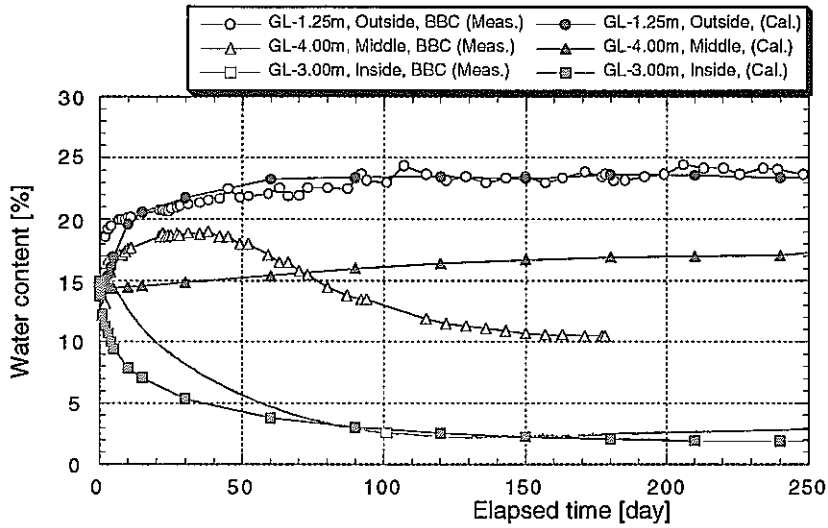

Figure 7-16 Comparison of water content in the buffer

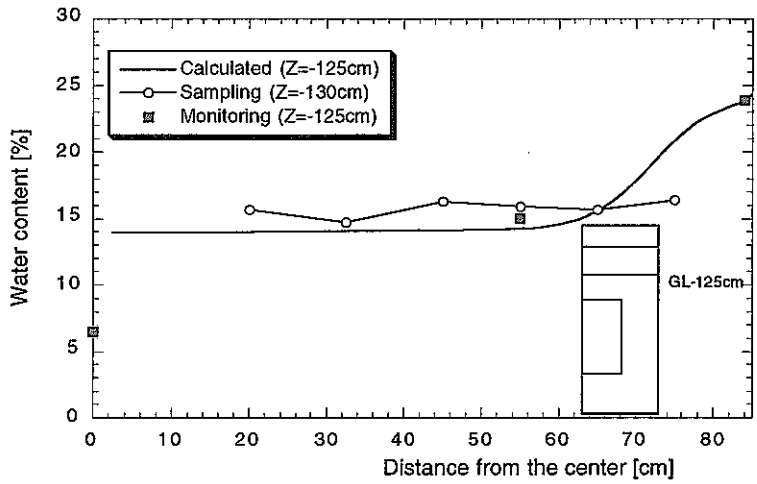

(a) GL -125 cm

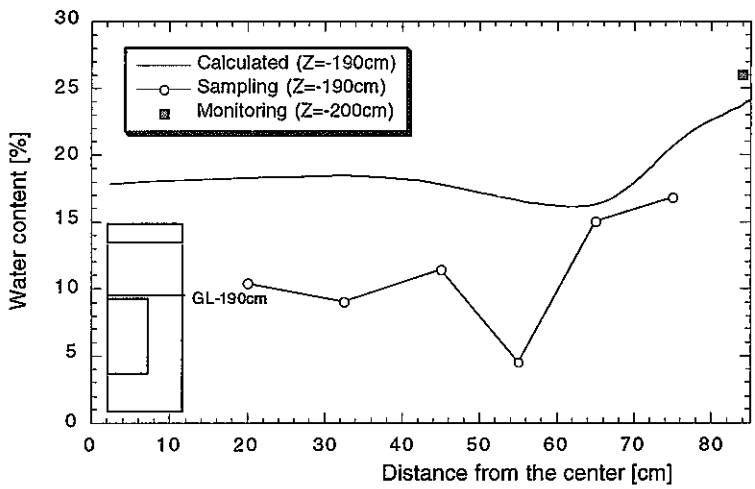

(b) GL -190 cm

Figure 7-17 Comparison of water content distribution at the end of heating phase

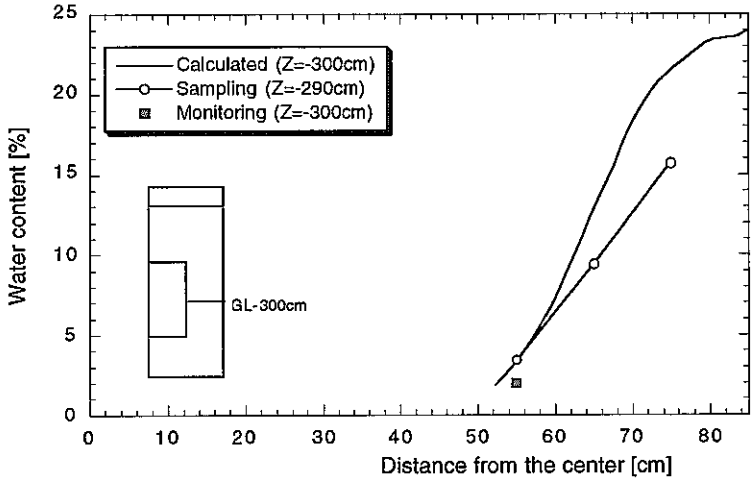

(c) GL -300 cm

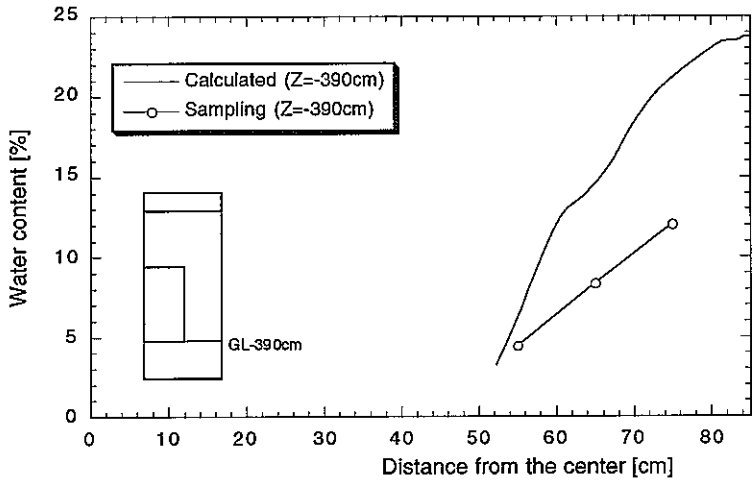

(d) GL -390 cm

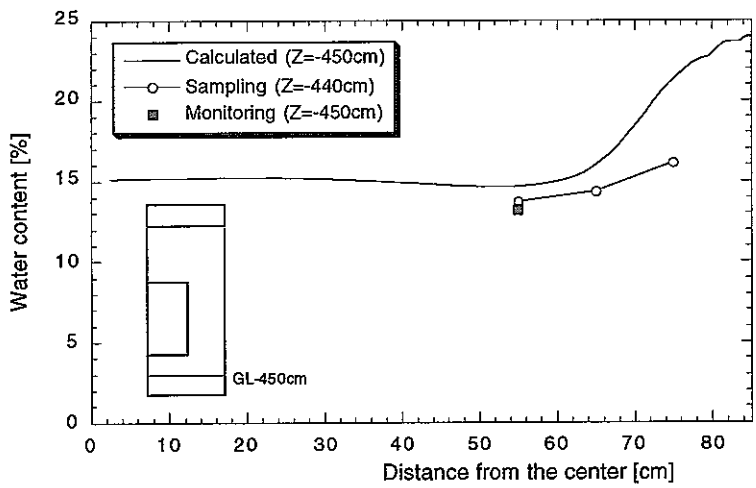

(e) GL -450 cm

Figure 7-17 Comparison of water content distribution at the end of heating phase (Contd.)

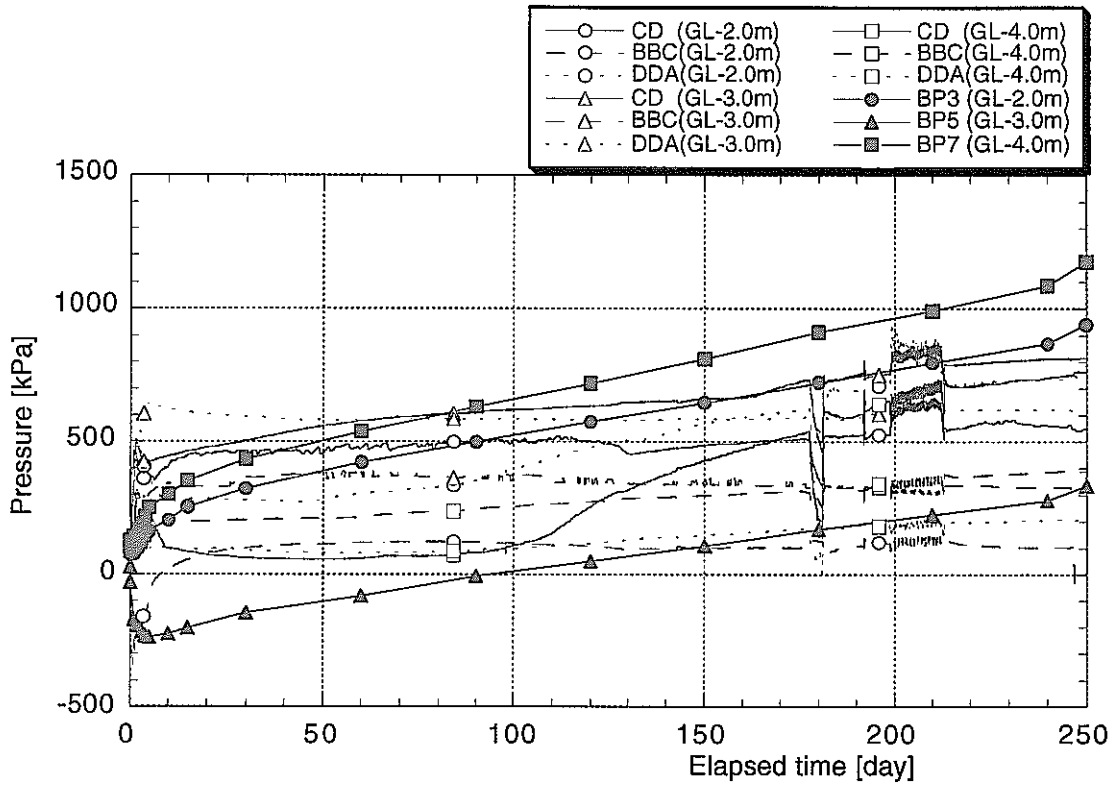

Figure 7-18 Comparison of total pressure during the heating phase

7.4 Confirmation of permeability of rock mass

In order to examine the effect of permeability of rock mass upon T-H-M phenomena in the buffer, sensitivity analyses on rock permeability are performed in this section. Test case is shown in Table 7-2. The hydraulic conductivity of rock mass in Case 1 is the same with geometric mean of measured hydraulic conductivity [Chijimatsu, M., et al., 1996]. The hydraulic conductivity of rock mass in Case 2 is one hundred times as large as geometric mean of measured hydraulic conductivity. The hydraulic conductivity of rock mass in Case 3 is one hundredth of geometric mean of measured hydraulic conductivity and that in Case 4 is almost the same with that of rock matrix. In Case 5, one horizontal fracture is considered as shown in Figure 7-19. The hydraulic conductivity of fracture is one thousand times as large as that of rock mass. The hydraulic conductivity of rock mass is the same with Case 1. The unsaturated properties of rock mass and fracture are the same one that is shown in Figure 7-2.

Figure 7-20 shows the time history of water content in the buffer. It can not seen the deference in water content according to permeability of rock mass even though there is fracture except for Case 4. It is because permeability of buffer is much lower than that of rock mass except for Case 4. If the hydraulic conductivity of rock mass is small and almost the same with the rock matrix and buffer, the water movement near the rock is slow because water outflow from the rock mass becomes very little. Figure 7-21 shows the time history of pore pressure at point KBH5-1. As the permeability of rock mass is small, pore pressure in rock mass decreases. However, the effect of this deference in pore pressure is small except for Case 4. Therefore, it is indicated that the effect of heterogeneity of rock permeability upon T-H-M phenomena in the buffer is small if the permeability of rock mass is enough larger than that of buffer mass.

Table 7-2 Permeability of test case

Hydraulic conductivity [cm/s]	Case 1	Case 2	Case 3	Case 4	Case 5
Rock mass	1.98×10^{-7}	1.98×10^{-5}	1.98×10^{-10}	1.98×10^{-11}	1.98×10^{-7}
Fracture	-	-	-	-	1.98×10^{-4}

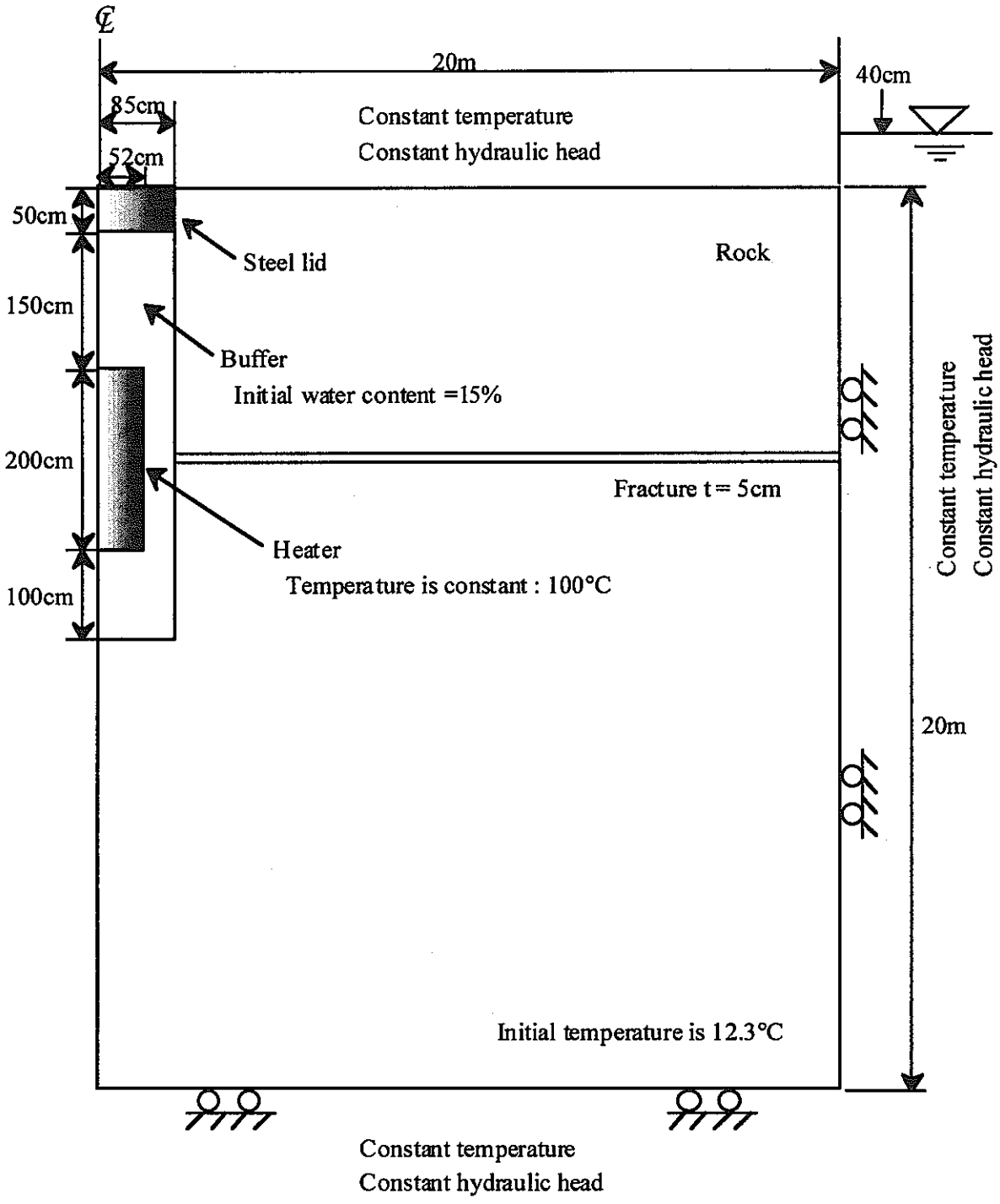

Figure 7-19 Model geometry including one fracture

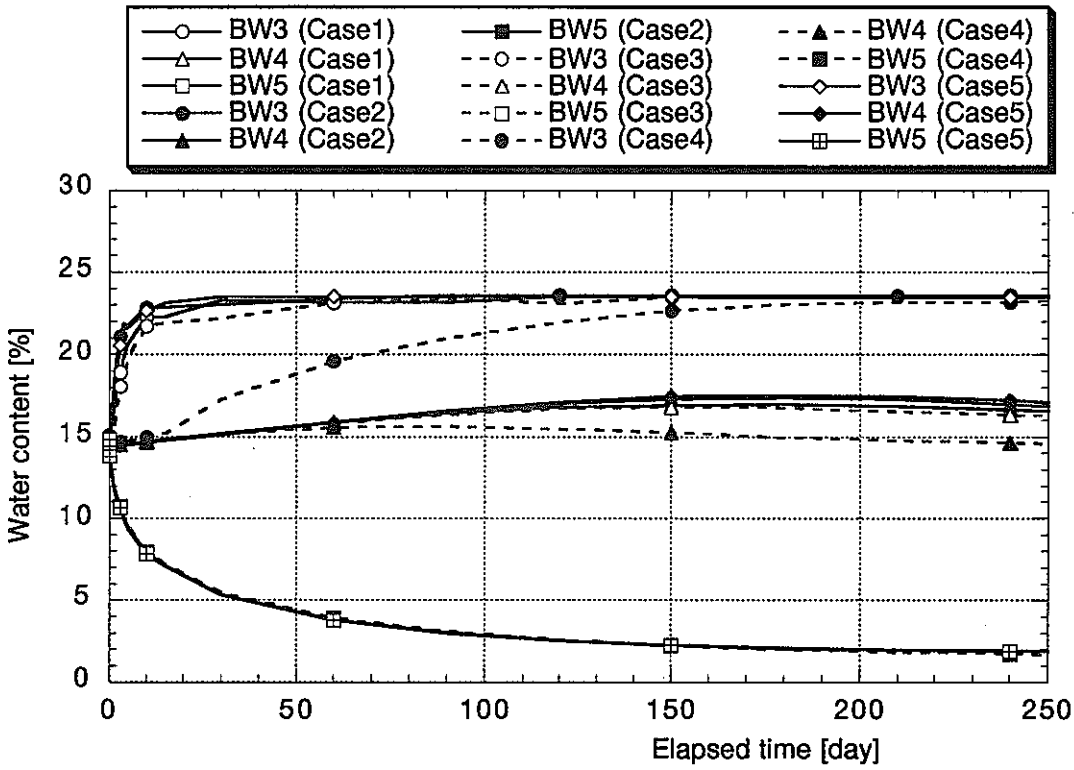

Figure 7-20 Effect of rock permeability on water content in the buffer

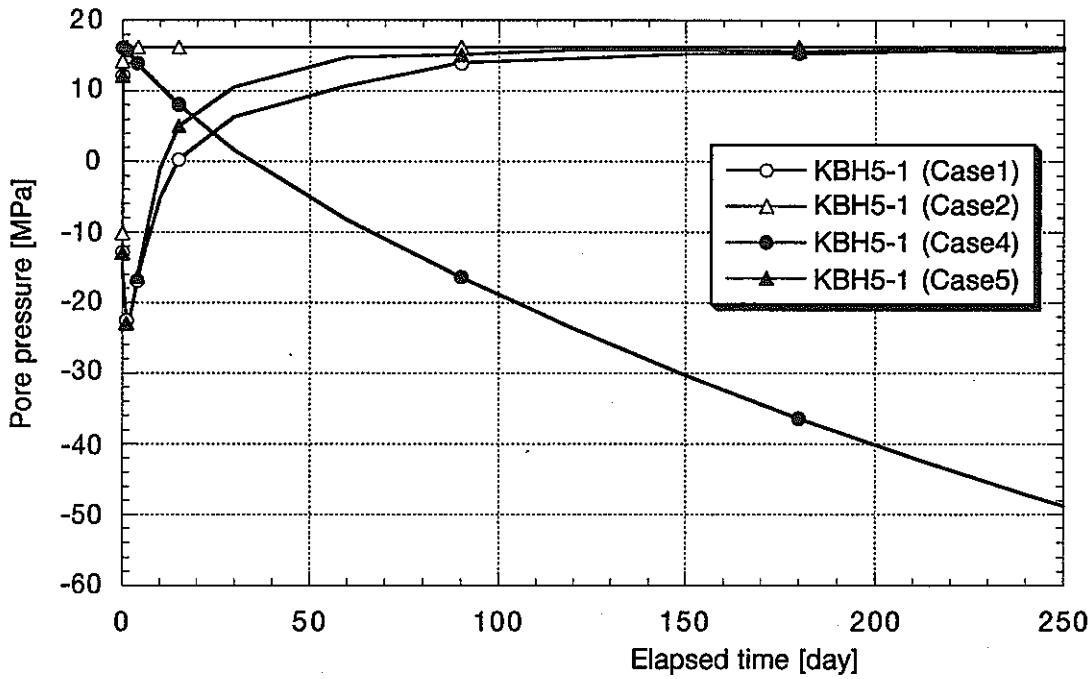

Figure 7-21 Effect of rock permeability on pore pressure in the rock mass

7.5 Analysis results (Cooling phase)

Figure 7-22 shows the calculated temperature distribution along the output line at the cooling phase. Distance expresses that from the center of the model. Temperature along the output line decreases gradually and becomes constant after 4 months from the stop of heating. Figure 7-23 shows the calculated water content distribution along the output line. Water content near the heater becomes high slowly. Figure 7-24 shows the distribution of water content in the buffer at the start of cooling phase and end of cooling phase (after 180 days). The water content near the heater is low when the cooling phase starts due to thermal gradient at the heating phase, and it increases during the cooling phase. However, the change of water content near the rock mass is not so much because the buffer near the rock mass is saturated during the heating phase.

Figures 7-25, 7-26, 7-27 and 7-28 show the comparison between the measured and calculated results. Figure 7-25 shows the comparison of temperature in the rock mass, (a) is at the borehole KBH5 and (b) is at the borehole KBH6. Figure 7-26 shows the comparison of temperature in the buffer, (a) is at the upper and lower part of buffer, (b) is at the center level of buffer. Figure 7-27 shows the comparison of water content in the buffer. Figure 7-28 shows the comparison of water content distribution at the end of cooling phase. Measured data were obtained by sampling and laboratory test at the 180 days passage from the start of cooling. A tendency of temperature rise and reduction of calculated results is almost same with measured. A tendency of water content change of calculated results is similar to the measured results. The water content distribution along GL -300 cm level is almost same between measured and calculated results. On the whole, calculated water content is good agreement with measured values.

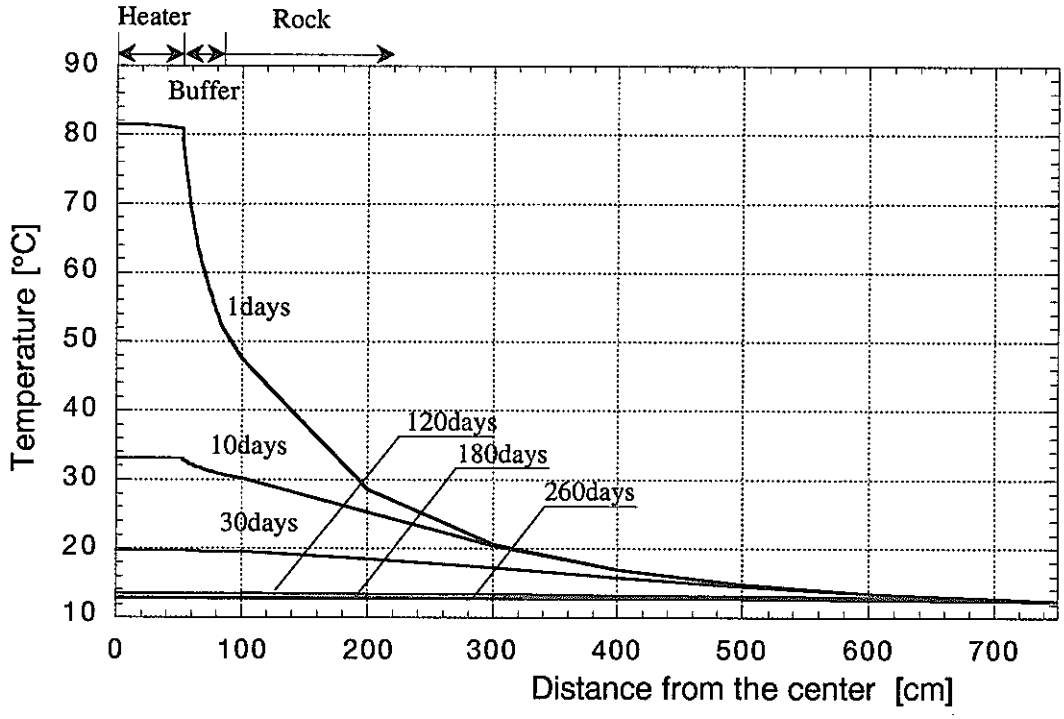

Figure 7-22 Temperature distribution along the Line I (Cooling phase)

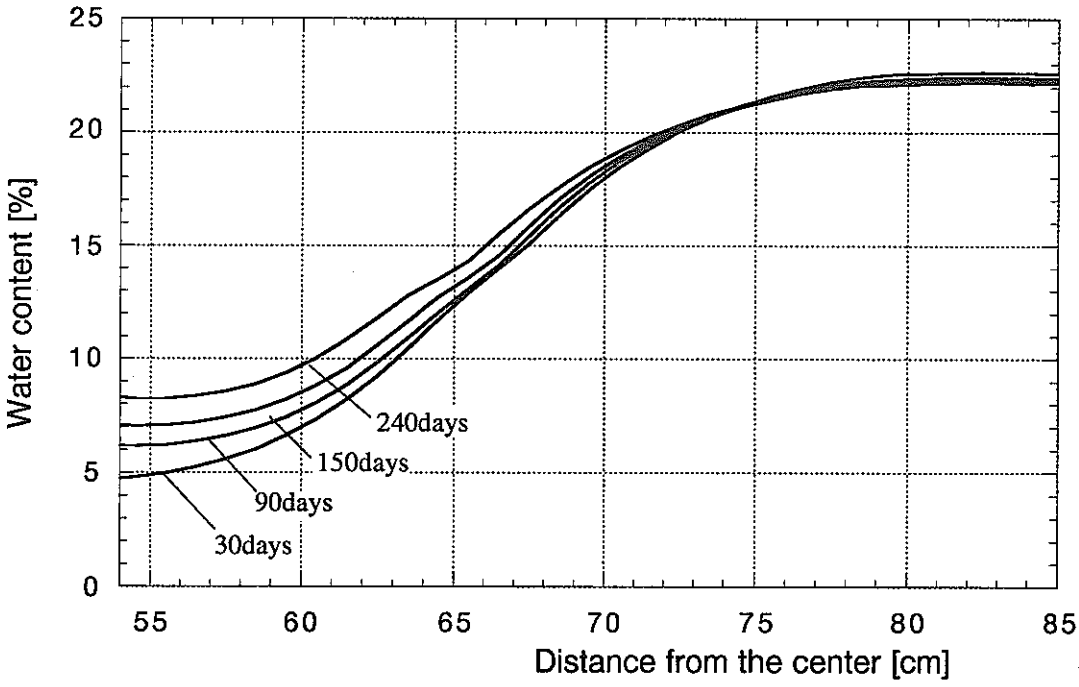

Figure 7-23 Water content distribution along the Line I (Cooling phase)

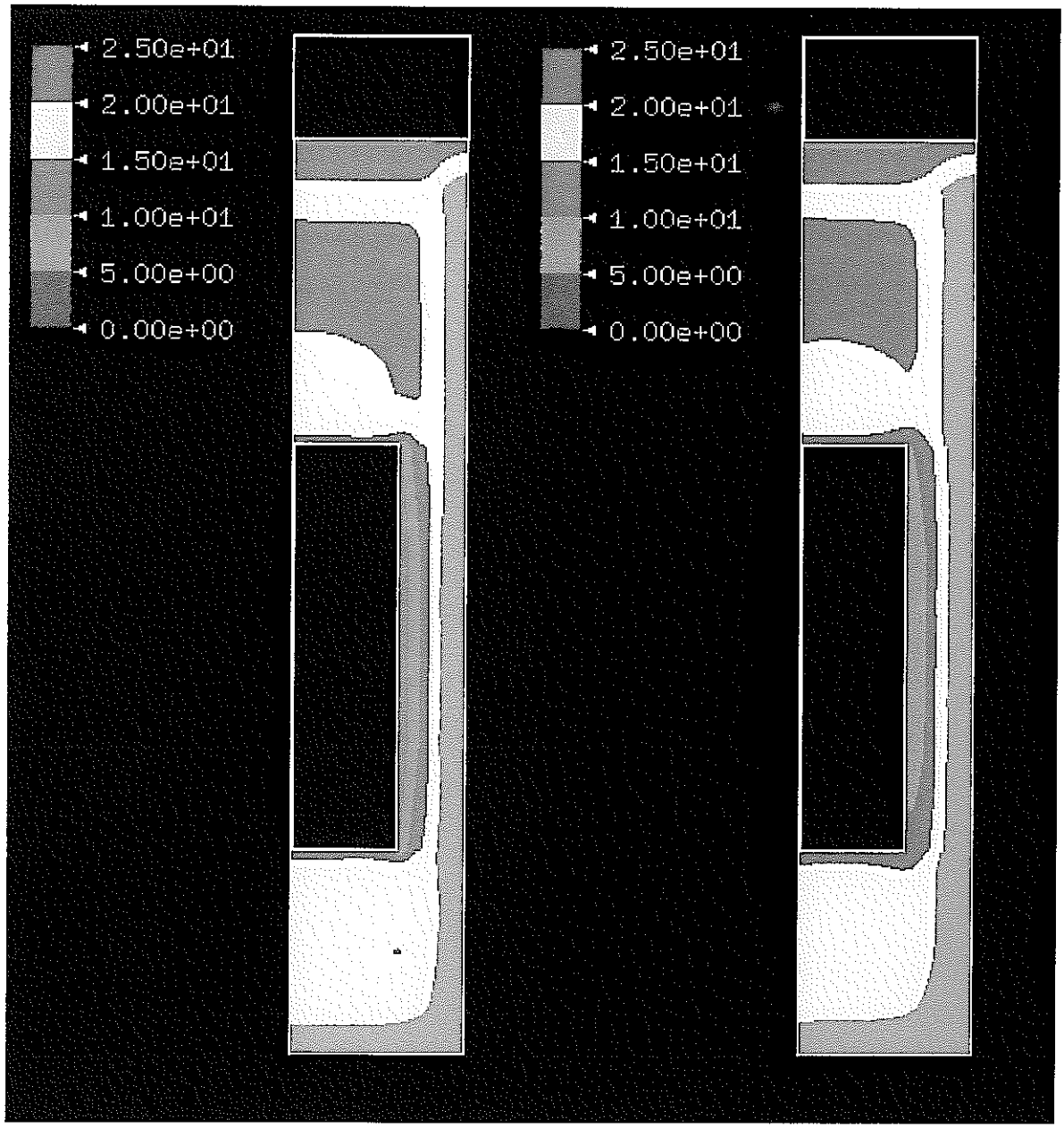

(a) Start of cooling phase (b) After 180 days

Figure 7-24 Water content distribution in the buffer material

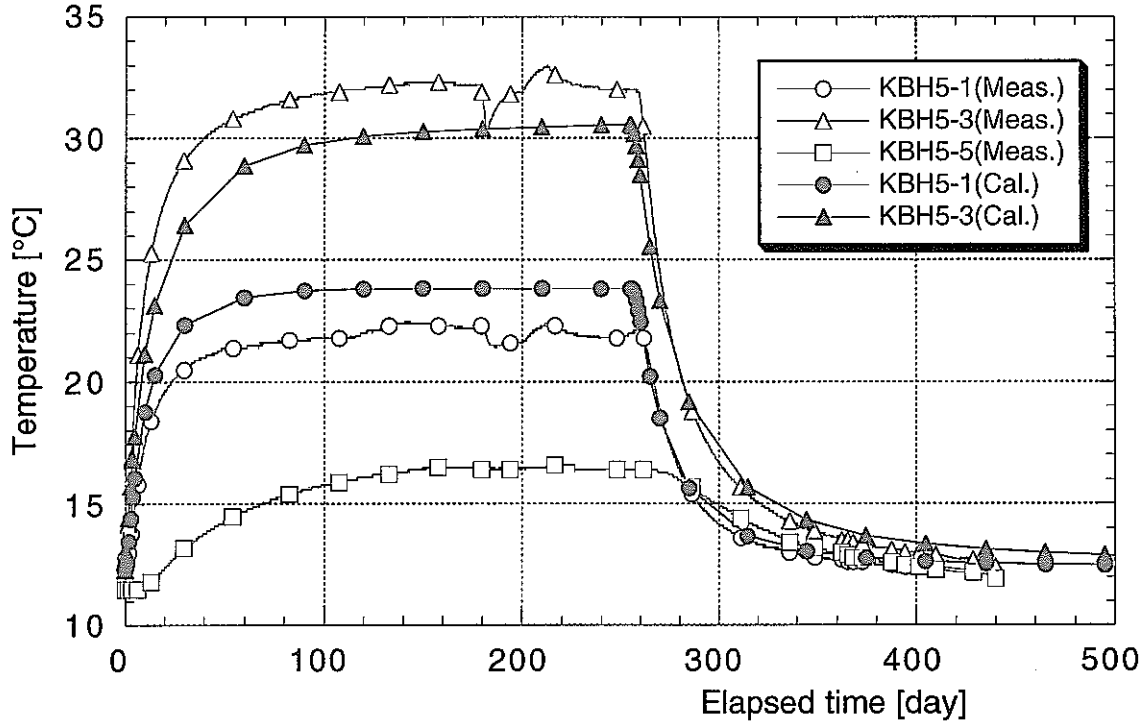

(a) KBH5

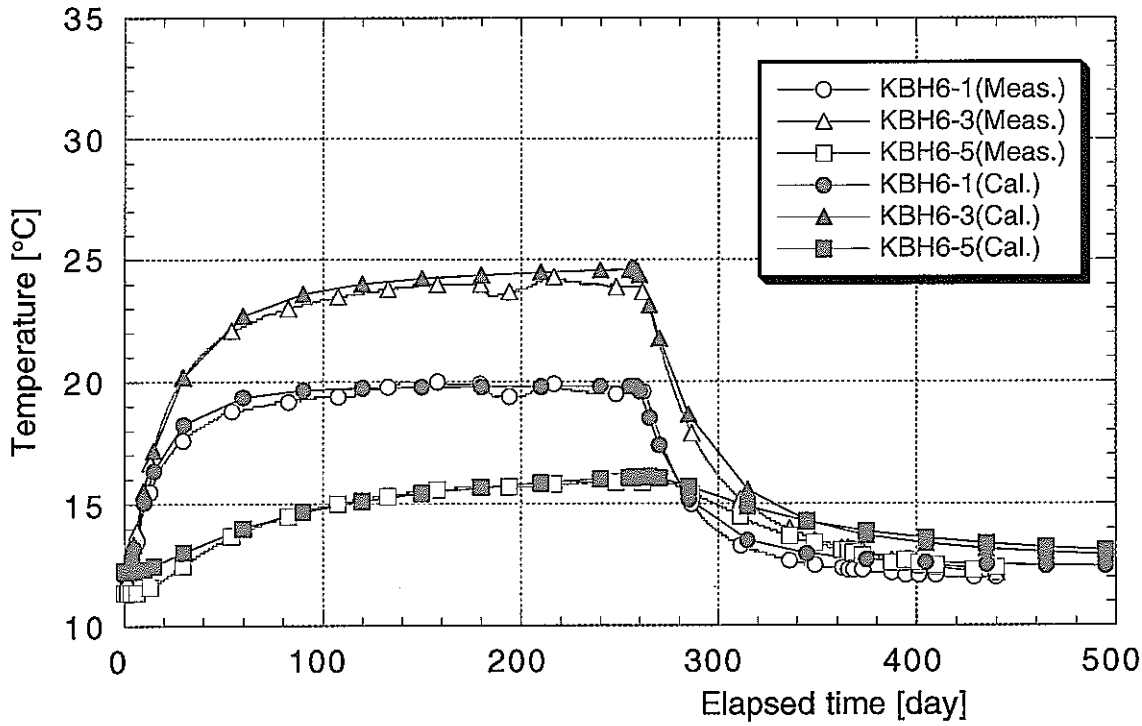

(b) KBH6

Figure 7-25 Comparison of the temperature in the rock mass
(Heating and Cooling phase)

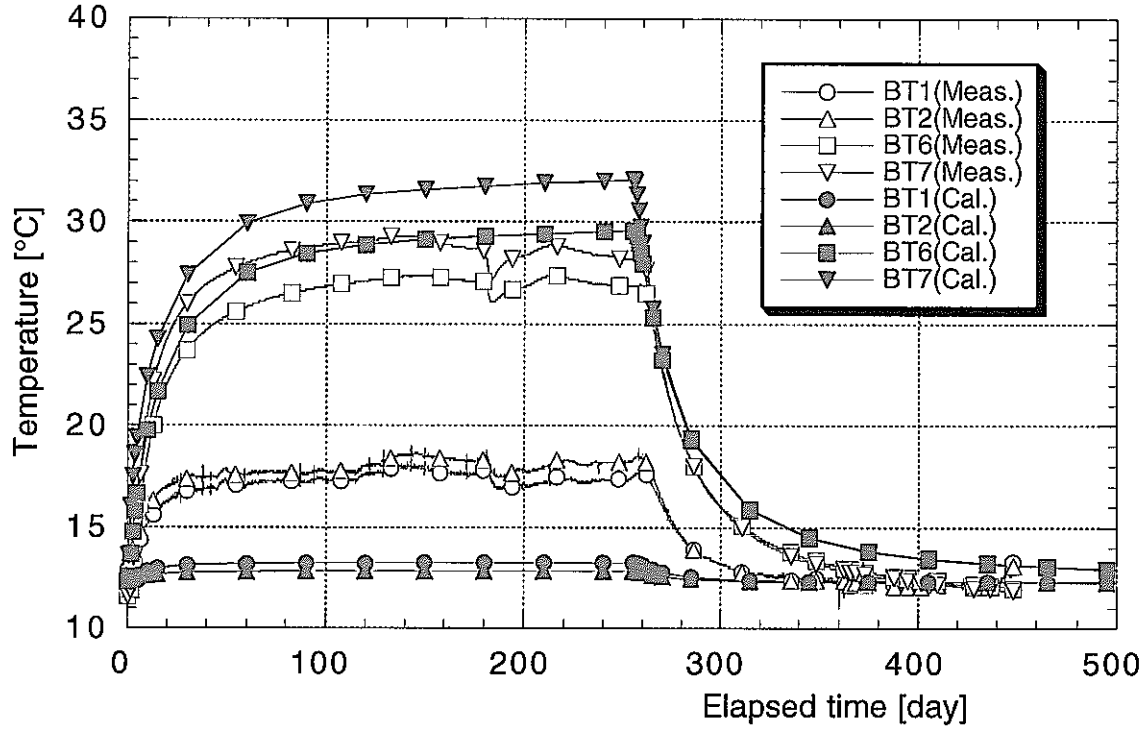

(a) Upper and Lower part of the buffer

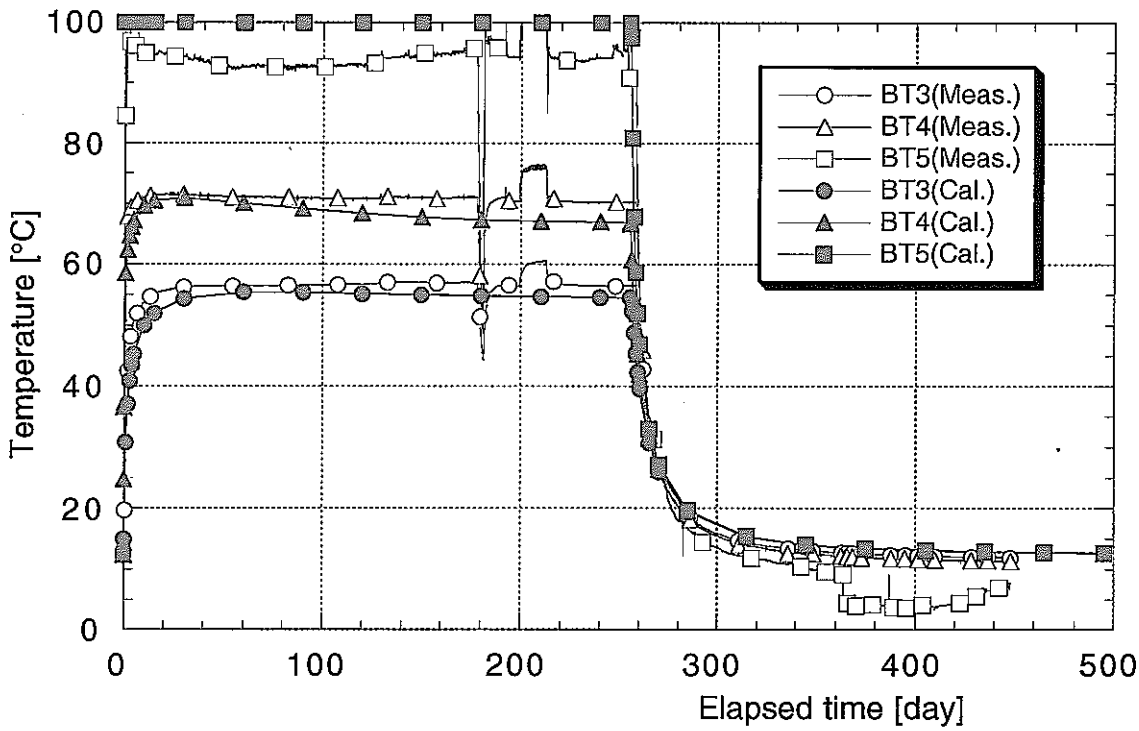

(b) Center level of the buffer

Figure 7-26 Comparison of the temperature in the buffer
(Heating and Cooling phase)

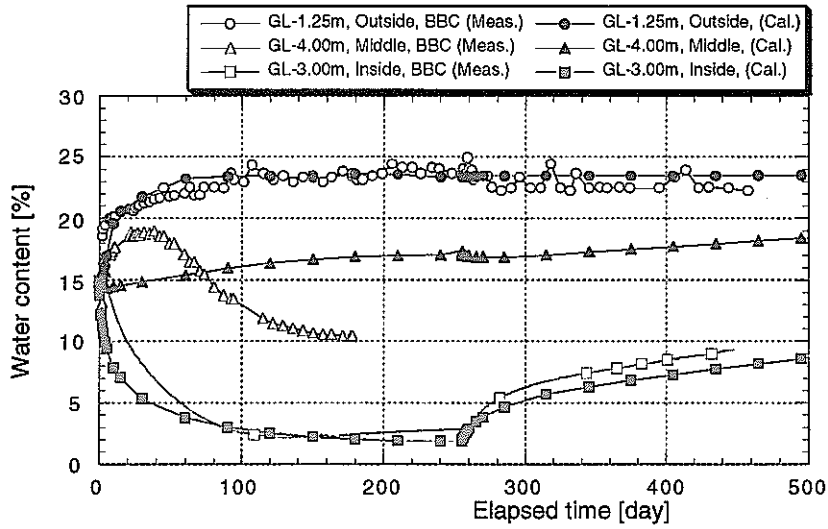

Figure 7-27 Comparison of water content in the buffer
(Heating and Cooling phase)

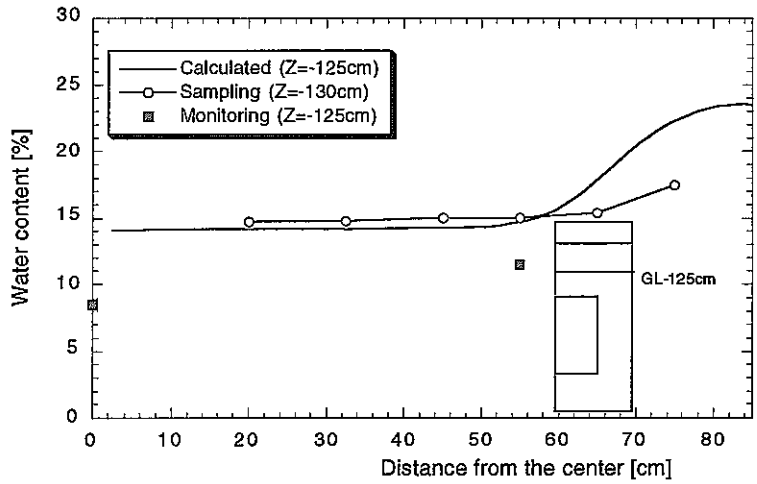

(a) GL -125 cm

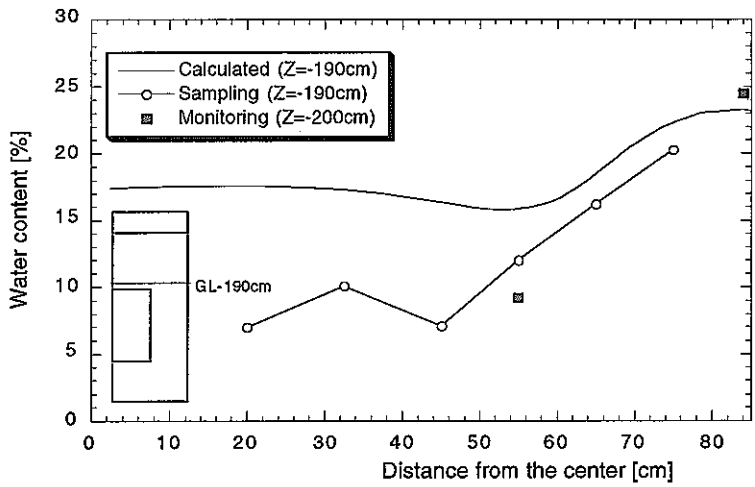

(b) GL -190 cm

Figure 7-28 Comparison of water content distribution at the end of cooling phase

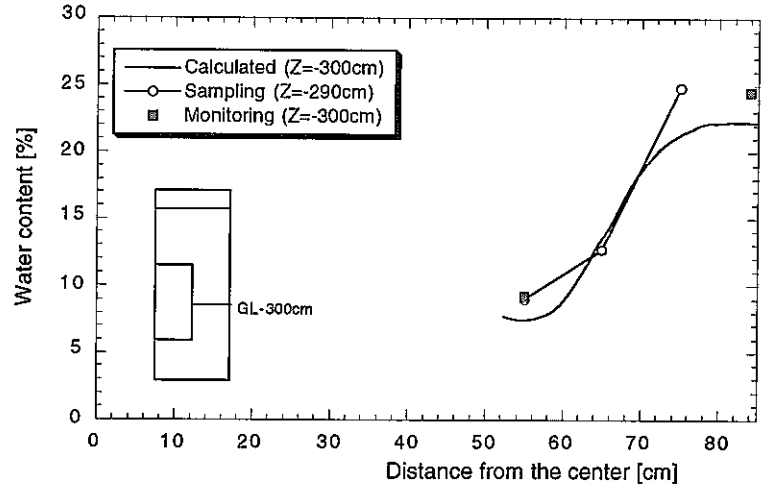

(c) GL -300 cm

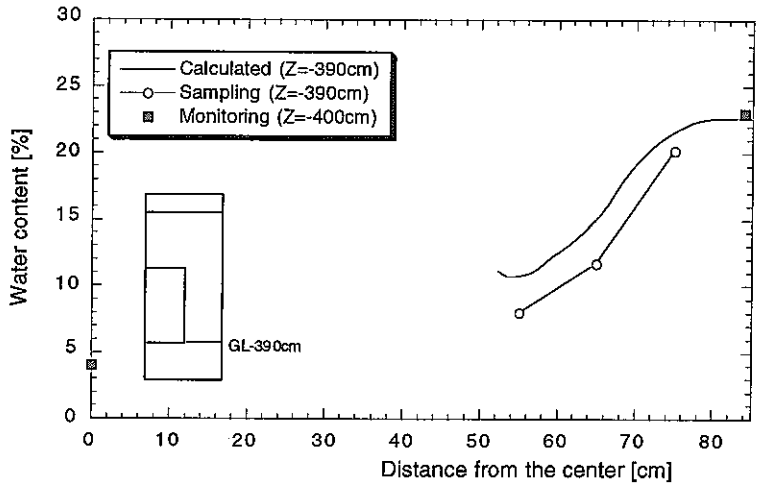

(d) GL -390 cm

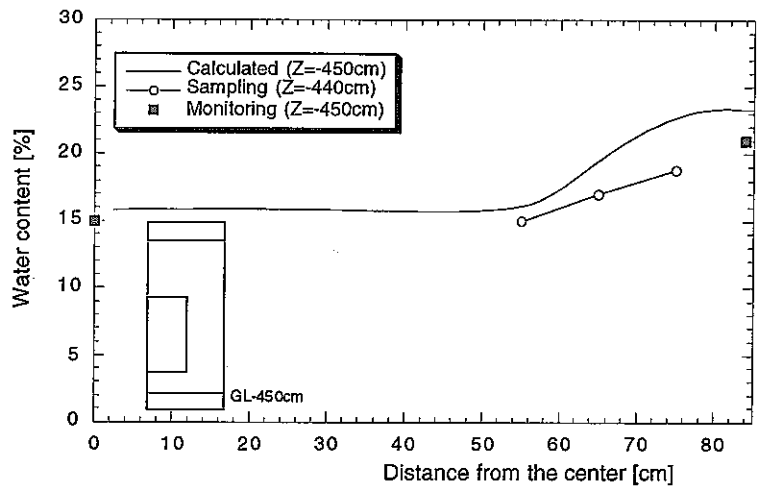

(e) GL -450 cm

Figure 7-28 Comparison of water content distribution at the end of cooling phase (Contd.)

7.6 Conclusions

In this section, the simulations of the coupled thermo-hydro-mechanical behavior in the near field were carried out by two dimensional model. The coupled T-H-M process was simulated with fully coupled calculation. The objective of this section is to estimate the T-H-M phenomena in the buffer and to confirm the effect of permeability of rock mass upon T-H-M phenomena in the buffer. From the results, the following conclusions are obtained.

(1) In the buffer material, temperature becomes constant at 30 days past from the start of heating, while, it takes about 150 days in the rock mass. Calculated temperature in the rock was higher than measured data. Calculated temperature in the buffer is in good agreement.
(2) Calculated water movement in the buffer is faster than measured one. At the steady state, calculated water content around the heater are in a good agreement with measured data, while calculated water content near rock mass is higher than measured data. It is considered that the reason of this discrepancy is due to use of inappropriate property of thermal water diffusivity or hydraulic property of rock mass and so on.
(3) Measured total pressure are between 0kPa and 500kPa, and become almost steady state at the early period. On the other hand, calculated total pressure become negative just after the start of heating and increase gradually because of the effect of swelling pressure. The use of unsuitable thermal expansion value of buffer material is considered to be the one cause of this discrepancy.
(4) The effect of heterogeneity of rock permeability upon T-H-M phenomena in the buffer is small if the permeability of rock mass is enough larger than that of buffer mass. Therefore, it can be concluded that the two-dimensional T-H-M analysis is enough if the main focus of the analysis is on the T-H-M phenomena in the buffer material.

Acknowledgment

The authors wish to express their gratitude to Prof. M. Nakano of Kobe University for kind and helpful advises on numerical methods. The authors are wishing to thank Dr. K. Amemiya of Hazama Corporation for his works of Kamaishi experiment. The authors are also wishing to thank Mr. H. Suzuki and Mr. K. Matsumoto of Inspection Development Corporation for their excellent technical assistance.

REFERENCE

Chijimatsu, M., T. Fujita, Y. Sugita, H. Ishikawa and A. Kobayashi; Coupled thermo-hydro-mechanical experiment at Kamaishi mine, Technical Note 07-95-07, Hydraulic Tests', PNC TN8410 96-058, Power Reactor and Nuclear Fuel Development Corporation, 1996.

Chijimatsu, M. , Y. Sugita, T. Fujita, and K. Amemiya; Coupled thermo-hydro-mechanical experiment at Kamaishi mine, Technical Note 15-99-02, Experimental Results', JNC TW8400 99-, Japan Nuclear Cycle Development Institute, 1999.

Decagon Device Inc.; SC-10A Thermocouple psychrometer sample changer operater's manual.

de Vries, D.A.; Heat transfer in soils. In Heat and Mass Transfer in the Biosphere. 1. Transfer Processes in Plant Environment (D.A. De Vries and N.H.Afghan, Eds.) New York; John Wiley & Sons Inc.,1974.

Fujita, T., Y. Sugita, T. Sato, H. Ishikawa and T. Mano; Coupled thermo-hydro-mechanical experiment at Kamaishi mine, Technical Note 01-95-01, Plan, PNC TN8020 94-005, Power Reactor and Nuclear Fuel Development Corporation, 1994.

Fujita, T., M. Chijimatsu, A. Kobayashi and Y. Ohnishi ; Coupled thermo-hydro-mechanical experiment at Kamaishi mine, Technical Note 10-96-03, Analyses of Task 2A, DECOVALEX III, PNC TN8410 97-026, Power Reactor and Nuclear Fuel Development Corporation, 1997a.

Fujita, T., M. Chijimatsu, H. Ishikawa, H. Suzuki and K. Matsumoto; Coupled thermo-hydro-mechanical experiment at Kamaishi mine, Technical Note 11-96-04, Fundamental properties of bentonite OT-9607, PNC TN8410 97-071, Power Reactor and Nuclear Fuel Development Corporation, 1997b.

Fujita, T., M. Chijimatsu, A. Kobayash, Y. Ohnishi and M. Tanaka; Coupled thermo-hydro-mechanical experiment at Kamaishi mine, Technical Note 13-98-01, Analyses of Task 2B, DECOVALEX III, PNC TN8410 98-079, Power Reactor and Nuclear Fuel Development Corporation, 1998.

Nakano, M., Y. Amemiya, K. Fujii, T. Ishida and Y. Ishii; Infiltration and expansive pressure in the confined unsaturated clay, Trans. Jpn. Soc. Irrig. Recalm.,112, 55-66,1984. (in Japanese)

Ohnishi, Y., H. Shibata and A. Kobayasi; Coupled Processes Associated with Nuclear Waste Repositories, edited by Tsang, C.F., pp. 679-697, 1989.

Philip, J.R. and de Vries,D.A.; Moisture movement in porous materials under temperature gradients, Am. Geophys. Union Trans, 38(2),pp.222-232.,1957

Stephansson, O., L. Jing and C.F. Tsang; Coupled thermo-hydro-mechanical processes of fractured media, Mathematical and experimental studies;, Developments in Geotechnical Engineering 79, Elsevier, 1996.

Suzuki, H., T. Fujita and T. Kanno; Water potential and water diffusivity of buffer material', PNC TN 8410 96-117, Power Reactor and Nuclear Fuel Development Corporation, 1996. (in Japanese)

Takeda, S. and H. Osawa; CURRENT STATUS AND FUTURE PROGRAM OF IN-SITU EXPERIMENTS OF KAMAISHI JAPAN, Proceedings of International Symposium on In-situ Experiments at Kamaishi, Nov.11-12, pp.IV-1-12, 1993.

Takeuchi, S., K. Hara and M. Nakano; Water retention curve, water diffusivity and water movement of compacted bentonite,Soil and Foundations, Japanese geotechnical Society, Vol.35, No.3,129-137,1995.(In Japanese)

van Genuchten, M.Th.; A closed-form equation for predicting the hydraulic conductivity of unsaturetaed soil, Soil Sci. Am. J., vol.44, No.5, 892-898, 1980.

Watanabe, K. ; Back analytical technique for evaluating the hydraulic parameters of unsaturated rock, 1991.

Yamato, A., S. Masuda and H. Sakuma ; High Level Radioactive Waste Management ; Proceedings of the 3rd International Conference, vol.1, pp.41-48, 1992.

Appendix

Tabulated data at the output points of Task 2C-2

Table A1 Temperature in the buffer [° C]

Elapsed time [day]	BT1	BT2	BT3	BT4	BT5	BT6	BT7
1	12.30	12.30	30.81	58.60	100.00	12.59	13.61
2	12.36	12.36	37.09	62.47	100.00	13.67	16.05
3	12.45	12.42	40.91	64.75	100.00	14.80	17.51
4	12.53	12.46	43.47	66.22	100.00	15.80	18.58
5	12.61	12.51	45.31	67.25	100.00	16.67	19.45
10	12.85	12.63	50.01	69.67	100.00	19.77	22.42
15	12.97	12.70	52.00	70.56	100.00	21.70	24.28
30	13.13	12.78	54.44	71.02	100.00	24.96	27.43
60	13.22	12.83	55.49	70.21	100.00	27.52	29.95
90	13.24	12.84	55.46	69.26	100.00	28.47	30.90
120	13.25	12.84	55.25	68.45	100.00	28.91	31.37
150	13.25	12.85	55.06	67.88	100.00	29.16	31.62
180	13.25	12.85	54.87	67.45	100.00	29.32	31.77
210	13.25	12.85	54.74	67.18	100.00	29.45	31.92
240	13.25	12.85	54.63	67.04	100.00	29.55	32.03
255	13.25	12.85	54.58	66.96	100.00	29.60	32.08
260	13.15	12.78	39.66	41.92	46.87	27.97	29.01
265	12.94	12.66	30.74	31.49	33.03	25.33	25.80
270	12.79	12.57	26.03	26.39	27.10	23.25	23.53
285	12.56	12.44	19.50	19.59	19.74	19.30	19.41
315	12.40	12.36	15.37	15.39	15.42	15.87	15.92
345	12.36	12.33	14.00	14.01	14.02	14.50	14.53
375	12.33	12.32	13.40	13.40	13.41	13.82	13.84
405	12.32	12.31	13.10	13.10	13.10	13.45	13.47
435	12.32	12.31	12.92	12.92	12.92	13.22	13.24
465	12.32	12.31	12.81	12.81	12.81	13.07	13.08
495	12.31	12.31	12.73	12.73	12.73	12.95	12.96
510	12.31	12.31	12.70	12.70	12.70	12.90	12.91
515	12.31	12.31	12.69	12.69	12.69	12.89	12.90

Table A2 Water content in the buffer [%]

Elapsed time[day]	BW1	BW2	BW3	BW4	BW5	BW6	BW7	BW8
0	15.00	15.00	15.00	15.00	15.00	15.00	15.00	15.00
1	14.80	14.87	16.11	14.46	12.25	14.73	14.70	14.55
2	14.93	14.82	17.76	14.46	11.34	14.89	14.63	14.47
3	15.44	14.80	18.89	14.48	10.70	15.44	14.59	14.43
4	16.15	14.78	19.82	14.51	10.00	16.17	14.55	14.41
5	16.93	14.76	20.62	14.54	9.47	16.99	14.52	14.39
10	19.62	14.70	22.25	14.67	7.87	19.74	14.43	14.33
15	20.59	14.66	22.26	14.80	7.09	21.01	14.38	14.37
30	21.78	14.54	23.31	15.14	5.35	22.57	14.27	14.48
60	23.30	14.45	23.16	15.83	3.79	23.61	14.22	14.71
90	23.45	14.36	23.15	16.42	3.01	22.80	14.18	14.94
120	23.49	14.27	23.56	16.76	2.54	23.66	14.15	15.15
150	23.33	14.20	23.58	16.87	2.25	22.39	14.17	15.35
180	23.66	14.14	23.58	16.95	2.06	23.68	14.21	15.50
210	23.61	14.09	23.59	16.83	1.94	23.67	14.25	15.62
240	23.43	14.04	23.58	16.64	1.88	23.67	14.31	15.73
255	23.47	14.19	23.58	16.85	1.90	23.58	14.65	16.28
260	23.45	14.16	22.92	16.39	2.93	23.40	14.64	16.15
265	23.50	14.17	22.78	16.30	3.48	23.38	14.70	16.16
270	23.51	14.19	22.76	16.31	3.87	23.38	14.74	16.17
285	23.49	14.21	22.63	16.31	4.67	23.36	14.82	16.16
315	23.53	14.24	22.46	16.42	5.70	23.37	14.91	16.10
345	23.53	14.26	22.40	16.65	6.33	23.36	14.98	16.05
375	23.52	14.29	22.35	16.87	6.85	23.36	15.03	16.00
405	23.53	14.31	22.30	17.06	7.33	23.36	15.08	15.95
435	23.53	14.36	22.26	17.24	7.79	23.36	15.13	15.90
465	23.54	14.43	22.22	17.42	8.21	23.36	15.17	15.85
495	23.54	14.49	22.18	17.59	8.64	23.35	15.22	15.81
510	23.54	14.52	22.16	17.68	8.84	23.35	15.25	15.78

Table A3 Void ratio in the buffer

Elapsed time[day]	BE1	BE2	BE3	BE4	BE5	BE6	BE7	BE8
0	0.6364	0.6364	0.6364	0.6364	0.6364	0.6364	0.6364	0.6364
1	0.6344	0.6337	0.6333	0.6326	0.6314	0.6328	0.6314	0.6303
2	0.6340	0.6332	0.6335	0.6318	0.6303	0.6322	0.6305	0.6292
3	0.6339	0.6328	0.6332	0.6310	0.6293	0.6317	0.6296	0.6281
4	0.6337	0.6323	0.6326	0.6302	0.6281	0.6313	0.6287	0.6270
5	0.6336	0.6318	0.6320	0.6293	0.6269	0.6309	0.6278	0.6259
10	0.6338	0.6313	0.6314	0.6283	0.6254	0.6310	0.6269	0.6247
15	0.6338	0.6308	0.6304	0.6273	0.6239	0.6304	0.6259	0.6236
30	0.6334	0.6303	0.6293	0.6261	0.6221	0.6306	0.6249	0.6223
60	0.6333	0.6297	0.6290	0.6248	0.6202	0.6297	0.6238	0.6210
90	0.6339	0.6291	0.6284	0.6234	0.6181	0.6294	0.6227	0.6197
120	0.6335	0.6286	0.6271	0.6220	0.6163	0.6288	0.6217	0.6185
150	0.6331	0.6281	0.6260	0.6206	0.6144	0.6285	0.6208	0.6173
180	0.6328	0.6276	0.6250	0.6192	0.6125	0.6279	0.6197	0.6160
210	0.6323	0.6271	0.6238	0.6178	0.6107	0.6271	0.6187	0.6148
240	0.6319	0.6266	0.6225	0.6165	0.6089	0.6265	0.6177	0.6136
250	0.6320	0.6261	0.6214	0.6151	0.6070	0.6261	0.6167	0.6124

Table A4 Total pressure in the buffer [MPa]

Elapsed time [day]	BP1	BP2	BP3	BP4	BP5	BP6	BP7	BP8
1	0.382	0.997	0.079	0.960	-0.170	1.083	0.144	1.328
2	0.454	1.071	0.096	0.963	-0.194	1.114	0.168	1.512
3	0.524	1.173	0.114	1.084	-0.215	1.230	0.191	1.766
4	0.594	1.282	0.137	1.192	-0.229	1.350	0.219	2.022
5	0.663	1.393	0.164	1.305	-0.237	1.472	0.252	2.331
10	0.739	1.569	0.206	1.501	-0.223	1.689	0.303	2.485
15	0.813	1.712	0.256	1.573	-0.202	1.832	0.355	2.879
30	0.892	1.842	0.324	1.786	-0.144	1.974	0.435	3.162
60	0.982	2.013	0.423	1.967	-0.079	2.155	0.540	3.602
90	1.072	2.158	0.501	2.126	-0.005	2.318	0.632	4.045
120	1.151	2.300	0.576	2.280	0.051	2.479	0.721	4.356
150	1.230	2.436	0.648	2.425	0.108	2.632	0.813	4.638
180	1.312	2.588	0.725	2.594	0.171	2.818	0.914	5.157
210	1.392	2.729	0.799	2.741	0.225	2.961	0.995	5.456
240	1.469	2.869	0.870	2.899	0.279	3.142	1.090	5.738
250	1.544	3.001	0.942	3.047	0.335	3.306	1.178	6.185

Table A5 Temperature in the rock mass [° C]

Elapsed time [day]	KBH5-1	KBH5-2	KBH5-3	KBH5-4	KBH6-1	KBH6-2	KBH6-3	KBH6-4	KBH6-5
1	12.56	15.83	13.01	12.30	12.25	11.30	12.23	12.30	12.30
2	13.46	19.42	14.43	12.30	12.25	11.64	12.23	12.30	12.30
3	14.41	22.06	15.71	12.33	12.46	12.68	12.49	12.31	12.30
4	15.29	24.08	16.82	12.41	12.80	13.85	12.89	12.33	12.30
5	16.06	25.69	17.78	12.53	13.20	14.98	13.35	12.39	12.30
10	18.77	30.46	21.14	13.40	15.09	19.14	15.55	12.97	12.35
15	20.28	32.84	23.16	14.32	16.36	21.56	17.21	13.72	12.49
30	22.34	36.08	26.44	16.44	18.26	25.13	20.23	15.59	13.04
60	23.47	37.94	28.89	18.56	19.38	27.41	22.71	17.58	14.02
90	23.75	38.36	29.73	19.49	19.67	28.06	23.61	18.47	14.67
120	23.83	38.43	30.08	19.97	19.76	28.28	24.01	18.94	15.12
150	23.85	38.42	30.27	20.27	19.79	28.38	24.24	19.23	15.44
180	23.84	38.37	30.38	20.48	19.80	28.41	24.39	19.44	15.67
210	23.84	38.34	30.47	20.64	19.81	28.44	24.49	19.59	15.86
240	23.83	38.32	30.54	20.76	19.81	28.46	24.58	19.72	16.01
255	23.83	38.30	30.57	20.82	19.81	28.47	24.62	19.77	16.08
260	22.47	33.08	28.51	20.78	19.61	27.99	24.39	19.77	16.10
265	20.22	27.75	25.58	20.38	18.53	25.29	23.15	19.54	16.11
270	18.52	24.33	23.33	19.74	17.40	22.90	21.77	19.08	16.06
285	15.65	18.97	19.19	17.85	15.19	18.51	18.64	17.50	15.70
315	13.69	15.23	15.70	15.56	13.52	15.10	15.59	15.42	14.89
345	13.05	13.95	14.35	14.47	12.97	13.90	14.33	14.41	14.30
375	12.78	13.37	13.70	13.89	12.73	13.35	13.72	13.85	13.89
405	12.64	13.08	13.35	13.54	12.61	13.07	13.38	13.52	13.60
435	12.57	12.91	13.14	13.31	12.54	12.91	13.17	13.30	13.39
465	12.52	12.80	13.00	13.15	12.50	12.80	13.02	13.14	13.23
495	12.48	12.72	12.89	13.03	12.46	12.72	12.92	13.02	13.10
510	12.47	12.69	12.85	12.98	12.45	12.69	12.87	12.97	13.05
515	12.46	12.68	12.84	12.96	12.45	12.68	12.86	12.96	13.03

Table A6 Pore pressure in the rock mass [kPa]

Elapsed time [day]	KBH5-1	KBH5-2	KBH5-3	KBH5-4	KBH6-1	KBH6-2	KBH6-3	KBH6-4	KBH6-5
1	-22.53	-10.10	-0.95	62.84	18.63	37.68	54.99	63.02	77.47
2	-22.19	-7.70	5.96	61.86	13.43	31.74	49.11	63.16	77.50
3	-19.50	-5.14	10.50	60.67	11.04	28.70	46.91	62.60	77.52
4	-16.92	-3.32	13.35	59.80	10.02	27.04	45.83	62.01	77.47
5	-14.53	-2.12	15.28	59.20	9.51	25.81	45.11	61.50	77.38
10	-5.22	4.38	21.46	57.82	9.19	18.83	42.08	60.07	76.92
15	0.29	8.17	24.24	57.76	9.93	18.45	40.62	59.64	76.64
30	6.29	11.94	28.48	58.27	11.74	19.95	40.56	59.47	76.29
60	10.71	18.66	35.47	59.35	12.74	24.98	45.11	59.99	76.13
90	14.00	29.05	43.15	59.92	13.48	30.34	47.58	60.41	76.18
120	14.56	30.69	44.96	60.78	14.06	31.33	48.25	61.04	76.40
150	15.27	32.84	46.80	61.65	14.47	32.54	49.44	61.72	76.65
180	15.31	32.39	46.56	61.68	14.60	32.75	49.67	61.91	76.81
210	15.65	33.00	46.67	61.69	14.65	32.75	49.54	61.87	76.84
240	16.04	33.55	47.67	62.24	14.88	33.22	50.11	62.26	76.99
255	15.91	33.30	47.48	62.10	14.85	33.17	50.06	62.24	77.02
260	15.76	33.08	47.53	62.21	14.81	33.16	50.10	62.27	77.03
265	15.82	32.93	47.53	62.31	14.84	33.16	50.17	62.35	77.06
270	15.77	32.88	47.52	62.37	14.82	33.09	50.18	62.41	77.09
285	15.58	32.54	47.24	62.26	14.68	32.83	50.03	62.38	77.14
315	15.45	32.35	47.18	62.30	14.54	32.62	49.92	62.36	77.20
345	15.38	32.27	47.13	62.27	14.48	32.54	49.86	62.33	77.22
375	15.36	32.24	47.10	62.25	14.47	32.50	49.83	62.31	77.22
405	15.40	32.25	47.11	62.25	14.47	32.51	49.83	62.31	77.23
435	15.38	32.24	47.10	62.25	14.47	32.50	49.82	62.31	77.23
465	15.40	32.26	47.13	62.27	14.48	32.52	49.84	62.33	77.24
495	15.44	32.30	47.17	62.29	14.50	32.55	49.87	62.35	77.25
510	15.44	32.29	47.17	62.29	14.50	32.55	49.87	62.35	77.26
515	15.44	32.30	47.18	62.29	14.50	32.55	49.87	62.35	77.26